LU TP 19-18
June 2019

PHENOMENOLOGY OF A THREE HIGGS DOUBLET MODEL WITH A $U(1) \times Z_2$ FLAVOUR SYMMETRY

Ian Padilla Gay

Department of Astronomy and Theoretical Physics, Lund University

Master thesis supervised by Roman Pasechnik and Dipankar Das
(30 credits)

LUND
UNIVERSITY

Abstract

We have studied the main features and the phenomenological consistency of a family-nonuniversal Three Higgs Doublet Model with a softly broken $U(1) \times Z_2$ family symmetry that enforces the flavour hierarchies in the Standard Model (SM) while implementing a tree-level Flavour Changing Neutral Current suppression in a Branco-Grimus-Lavoura way. Furthermore, the alignment limit is imposed in the scalar sector to enforce the physical scalar spectrum to accommodate a SM-like Higgs boson. To verify the consistency of our model, we have performed numerical analyses to confront experimental data coming from Higgs searches, electroweak precision tests and quark flavour violating (QFV) processes. We conclude that the model studied in this thesis is capable of suppressing dangerous FCNCs mediated by non-SM scalars. Furthermore, some scalars are found to be relatively light suggesting that the model succeeds in confronting flavour data even in the presence of scalars with masses around 300 GeV. Hence, the 3HDM presented in this thesis opens the door to direct searches for non-SM scalars at future runs of the LHC.

Popular science abstract

The Standard Model of Particle Physics represents the most complete and predictive model of particle physics that attempts to describe the interactions between the fundamental blocks of nature, such as leptons and quarks interacting with the Higgs boson. Although the Standard Model has proven to be a powerful tool for describing almost all current observations in particle physics, it still lacks strong arguments to explain the free parameters and the different hierarchies that appear for no clear reason. For a long time, many different types of models have been proposed to alleviate the lack of information that the SM offers about the origin of the masses and mixing angles. Motivated by this goal, it is crucial to further propose new models and verify if their predictive power is sufficient to become a strong candidate for a model that goes beyond the Standard Model. This thesis consists of verifying the consistency of a new type of Three Higgs Doublet Model, which could possibly shed light on some of the mysterious features of the Standard Model and unravel potential new physics.

Contents

1 Introduction

The Standard Model (SM) is currently the most successful theory of particle physics capable of describing masses of bosons and fermions as well as the interactions between them and with the Higgs boson. Great efforts have been put into the study of the SM phenomenology at large collider experiments in order to verify our understanding of the particle content and interactions in nature. The last missing piece was the discovery of the Higgs boson at LHC, with a mass of roughly 125 GeV [1], whose decays have been measured with high accuracy. This remarkable discovery is firm evidence that at least one Higgs doublet is needed to account for, firstly, the breaking of the electroweak (EW) $\mathrm{SU(2)_L \times U(1)_Y}$ symmetry down to $\mathrm{U(1)_{EM}}$ electromagnetic symmetry, and secondly, the origin of masses of gauge and fermion fields. Despite a remarkable consistency with the wealth of experimental measurements, the SM still remains an incomplete framework that fails to explain some of the fundamental features of particle spectra and interactions from a theoretical perspective.

Models with non-minimal Higgs sectors play an important role in the search of physics Beyond the Standard Model (BSM) [2]. The incorporation of additional Higgs boson states into the scalar sector helps to mitigate some of the difficulties in the SM framework and offers a rich phenomenology that can be tested at current collider experiments. Some of the undesired and profoundly rooted difficulties of the SM are supported by overwhelming evidence; it fails to accommodate Dark Matter and to explain the large baryon asymmetry in the Universe, which are very well tested facts in astrophysics and cosmology. Also, the Yukawa sector remains unmotivated by any fundamental symmetry and no theoretical justification exists for its origin or its free parameters. Besides, the Yukawa sector is plagued by hierarchies e.g. the mass of the t quark is thousands of times greater than the u quark for no clear reason. The mixing of quarks could not be rescued from a hierarchical structure either: the Cabibbo–Kobayashi–Maskawa matrix (CKM) has small but not-vanishing off-diagonal entries which have been measured with high accuracy through the decays of B, D and K mesons, confirming a hierarchical pattern in the mixing of quarks.

The simplest extension is the Two Higgs Doublets Model (2HDM) which incorporates extra charged and neutral scalar fields by adding a second $\mathrm{SU(2)_L}$ Higgs doublet to the SM Lagrangian. This type of models has been extensively studied in the literature [3][4]. Despite their rich phenomenology, this type of minimal models has the undesired feature of showing Flavour Changing Neutral Currents (FCNC) at tree-level, which naturally emerge since in general diagonalization of mass matrices does not lead automatically to diagonal Yukawa matrices. Thus, the off-diagonal terms of the Yukawa matrices will allow flavour changing interactions of fermions at tree-level, which are not observed at that order of perturbation theory. Consequently, FCNCs need be suppressed by some mechanism, typically, by very large energy scale of new physics (NP) or by small couplings of NP to the SM sectors.

A particular multi-Higgs extension has been pursued in this project by examining the phenomenology of a Three Higgs Doublet Model (3HDM) with a softly-broken $\mathrm{U(1)} \times \mathrm{Z_2}$ symmetry in the scalar and flavour sector of the Lagrangian. We offer a 3HDM where the fermion hierarchies are, at least, partially related to the hierarchies in the Higgs Vac-

uum Expectation Values (VEVs). This thesis project is built upon a previously proposed 3HDM scenario presented by the authors in reference [5] and provides some improvements with respect to the original formulation of the model. One crucial difference between the aforementioned model and the one presented in this thesis is the incorporation of a realistic CKM matrix. Nevertheless, this improvement comes at the expense of tree-level FCNCs which are absent in the model in [5]. The main goal of this thesis is to build a 3HDM capable of reproducing the quark mixing patterns in the CKM matrix while suppressing potentially dangerous tree-level FCNCs that could emerge in the model. This is a bottom-up approach for the search of NP where efforts are focused on the features of the theory at the EW scale incorporating the plentiful experimental constraints coming from Higgs and flavour physics. To better understand the model analyzed in this thesis, we present an overview of the SM including a description of its most important meson processes together with a discussion of where NP might have a significant effect.

The outline of this thesis project looks as follows. First, in section 2 we present some of the main features of the SM needed to discuss flavour physics in the context of models with extended Higgs sectors such as 3HDMs. In particular, rare K meson decays and B meson physics are discussed since they can deliver interesting signatures of NP. Then, in section 3 we introduce and discuss in detail our flavoured 3HDM with special emphasis on the new tree- and loop-level interactions (not present in the SM), which are mediated by exotic scalars in our 3HDM. Lastly, in sections 4 and 5 we present the results of our scans where we check for the phenomenological consistency of our model and conclude on the potentially viable regions of its parameter space.

2 The Standard Model

To pave the way towards a model with an extended Higgs sector, let us revisit the main features of the SM [6][7][8][9].

2.1 Internal symmetry

The SM is a spontaneously broken non-abelian gauge theory with the following gauge symmetry group,

$$\mathrm{SU(3)_C} \times \mathrm{SU(2)_L} \times \mathrm{U(1)_Y}. \tag{2.1}$$

Given this symmetry, the SM describes the electroweak- and strong forces based on gauge invariance. The $\mathrm{SU(3)_C}$ symmetry, which remains unbroken, corresponds to Quantum Chromodynamics (QCD) and describes strongly interacting particles. On the other hand, the $\mathrm{SU(2)_L} \times \mathrm{U(1)_Y}$ symmetry, which is spontaneously broken through the Higgs mechanism, is responsible for EW interactions.

Fermions come in three copies (generations) of the following representations

$$\left(1, 2, -\frac{1}{2}\right) \oplus \left(1, 1, +1\right) \oplus \left(3, 2, +\frac{1}{6}\right) \oplus \left(\overline{3}, 1, -\frac{2}{3}\right) \oplus \left(\overline{3}, 1, +\frac{1}{3}\right) \tag{2.2}$$

and a scalar field (Higgs boson) in the $\left(1, 2, \frac{1}{2}\right)$ representation. In (2.2), we refer to the direct sum of individual subspaces that constitute the SM representation. The hypercharge is given in the third entry of each triplet, while the color charge and the $\mathrm{SU(2)_L}$ weak isospin are given in the first and second entry, respectively. In order of appearance in (2.2) multiplets correspond to the following fields: $e_L, \overline{e}_R$, u_L (and d_L), $\overline{u}_R, \overline{d}_R$, respectively. The SM group representation specifies the $\mathrm{SU(3)_C}$ color representation, in which leptons are singlets and quarks are color triplets (or color anti-triplet for anti-quarks). Similarly, one has the $\mathrm{SU(2)_L}$ group, in which right-handed (R-handed) particles are singlets and left-handed (L-handed) are doublets. The scalar field of the SM, the Higgs boson, is a $\mathrm{SU(2)_L}$ doublet with $+1/2$ hypercharge and a color singlet.

Interactions are included in the SM through the gauge invariance of the SM Lagrangian $\mathcal{L}_{\mathrm{SM}}$. At the Lagrangian level, gauge interactions are introduced by the gauge covariant derivative,

$$D_\mu = \partial_\mu - ig'\frac{Y}{2}B_\mu - ig\frac{\tau^i}{2}W_\mu^i - ig_C\frac{\lambda^a}{2}G_\mu^a, \tag{2.3}$$

written in terms of the generators of the symmetries of the SM. In the EW sector there are four generators W_μ^i, B_μ which give rise to the weakly interacting vector bosons $W^\pm, Z^0$ and the electromagnetic vector boson γ, the photon. In the color sector, there are eight generators G_μ^a that correspond to eight gluons g^a mediating strong interactions. The introduction of the gauge covariant derivative has a twofold consequence. First, it ensures that the $\mathcal{L}_{\mathrm{SM}}$ is invariant under gauge transformations, and second, it introduces the interactions of fields through the presence of the gauge bosons.

Despite the success of the SM, an explanation for the origin of its internal symmetries still does not exist even though a great amount of reactions governed by these symmetries have been thoroughly studied at collider experiments. Equally puzzling is the question of why nature has chosen these particular symmetries and whether a larger symmetry, which contains the SM, remains to be discovered. We will however not attempt to address these puzzles in this work, instead we focus our efforts on reproducing the mass and mixing patterns in the flavour sector of the SM.

2.2 Electroweak interactions

The description of weak interactions and electromagnetism is achieved by the Higgs mechanism of the SSB of $\mathrm{SU(2)_L \times U(1)_Y \to U(1)_{EM}}$. R-handed fermions transform as singlets while the L-handed leptons and quark fields as doublets under $\mathrm{SU(2)_L}$

$$\Psi_i = \begin{pmatrix} \nu_i \\ \ell_i^- \end{pmatrix}, \quad Q_i = \begin{pmatrix} u_i \\ d_i \end{pmatrix}, \tag{2.4}$$

where the subindex i refers to the i-th family. In the SM, the VEV of the complex scalar Higgs doublet $H = \begin{pmatrix} H^+ \\ H^0 \end{pmatrix}$ breaks the $\mathrm{SU(2)_L \times U(1)_Y}$ symmetry of the vacuum accounting

for mass generation of gauge bosons and fermions. The SM scalar potential is given by

$$V(\phi) = -\mu^2 H^\dagger H + \frac{\lambda^2}{2}(H^\dagger H)^2, \tag{2.5}$$

where the VEV v obeys the relation $v/\sqrt{2} = \mu/\lambda$ and is measured to be $v \approx 246$ GeV. After SSB, only one neutral scalar Higgs scalar h remains physical and the Lagrangian for fermions fields ψ_i takes the following form

$$\begin{aligned}\mathcal{L}_F = &\sum_i \overline{\psi}_i\Big(i\gamma^\mu\partial_\mu - m_i - \frac{m_i h}{v}\Big)\psi_i - \frac{g}{2\sqrt{2}}\sum_i \overline{\Psi}_i\gamma^\mu(1-\gamma^5)(T^+W_\mu^+ + T^-W_\mu^-)\Psi_i \\ &- e\sum_i Q_i\overline{\psi}_i\gamma^\mu\psi_i A_\mu - \frac{g}{2\cos\theta_W}\sum_i \overline{\psi}_i\gamma^\mu(g_V^i - g_A^i\gamma^5)\psi_i Z_\mu,\end{aligned} \tag{2.6}$$

where $T^\pm$ are the weak isospin ladder operators, $\theta_W \equiv \tan^{-1}(g'/g)$ is the weak mixing angle, $e = g\sin\theta_W$ the electric charge of e^+, A is the photon field (γ) and $Z, W^\pm$ are the neutral and charged weak bosons. The EW bosons in the gauge basis are related to the physical gauge bosons through the following rotations

$$Z^{\gamma Z} = \begin{pmatrix} \cos\theta_W & -\sin\theta_W \\ \sin\theta_W & \cos\theta_W \end{pmatrix}, \quad Z^W = \begin{pmatrix} \frac{1}{\sqrt{2}} & i\frac{1}{\sqrt{2}} \\ -i\frac{1}{\sqrt{2}} & \frac{1}{\sqrt{2}} \end{pmatrix}. \tag{2.7}$$

With these definitions, the change of basis reads as follows

$$\begin{pmatrix} B_\mu \\ W_\mu^3 \end{pmatrix} = Z^{\gamma Z}\begin{pmatrix} \gamma_\mu \\ Z_\mu \end{pmatrix}, \quad \begin{pmatrix} W_\mu^1 \\ W_\mu^2 \end{pmatrix} = Z^W\begin{pmatrix} W_\mu^+ \\ W_\mu^- \end{pmatrix}. \tag{2.8}$$

The EW bosons Z, γ and $W^\pm$ will mediate the *neutral* and *charged* currents. For instance, the second term in the fermion Lagrangian $\mathcal{L}_F$ allows electrons and neutrinos to couple to the weak W boson through a charged current interaction. Similarly, up-type and down-type quarks participate in EW reactions with a coupling controlled by the CKM elements as will be outlined below. In summary, weak interactions are peculiar for two reasons. Firstly, they change the quark- and lepton flavour through charged currents and secondly, they do not only violate parity symmetry but also charge-parity ($\mathcal{CP}$) symmetry; apart from QCD interactions, this $\mathcal{CP}$-violation is only possible in the EW sector of the SM. The study of charged currents will become central when discussing *flavour* physics and ongoing NP searches.

2.3 Yukawa sector

All fundamental matter fields come in three generations. They share the same conserved charges and can be grouped in families with increasing masses. The non-universality of flavour interactions is encoded in the quark Yukawa sector of the SM, $\mathcal{L}_\text{Y}$, where quarks couple to the Higgs field acquiring mass through the Higgs mechanism. If leptons are

included in the description and neutrinos are assumed to be massless, fermion interactions with the Higgs doublet are contained in

$$\mathcal{L}_{\mathrm{Y}} = -Y^{d}_{ij}\overline{Q}_{Li}Hd_{Rj} - Y^{u}_{ij}\overline{Q}_{Li}\epsilon H^{*}u_{Rj} - Y^{e}_{ij}\overline{\Psi}_{Li}He_{Rj} + h.c., \tag{2.9}$$

where $Y^{u,d,e}$ are 3×3 (complex) Yukawa matrices, H as defined in the previous section and $\epsilon = i\sigma_2$[1] which ensures that ϵH^* transforms in the same way as H under $\mathrm{SU(2)_L}$. The indices $i, j = 1, 2, 3$ correspond to three families of fermions. Here Q_{Li}, L_{Li} and d_{Ri}, u_{Ri}, e_{Ri} are the $\mathrm{SU(2)_L}$ doublets and singlets, respectively. In the quark sector, mass matrices for the quarks are generated after SSB via the Higgs mechanism,

$$\mathcal{L}_{\mathrm{Y}} = -Y^{d}_{ij}\begin{pmatrix}\overline{u}_L & \overline{d}_L\end{pmatrix}_i\begin{pmatrix}0\\ \frac{v}{\sqrt{2}}\end{pmatrix}d_{Rj} - Y^{u}_{ij}\begin{pmatrix}\overline{u}_L & \overline{d}_L\end{pmatrix}_i\begin{pmatrix}\frac{v}{\sqrt{2}}\\ 0\end{pmatrix}u_{Rj} + h.c.. \tag{2.10}$$

The mass matrices for the up-type and down-type quarks have been expressed in terms of generic 3×3 complex Yukawa matrices and the VEV of the Higgs doublet,

$$M^{u}_{ij} = Y^{u}_{ij}\frac{v}{\sqrt{2}}, \quad M^{d}_{ij} = Y^{d}_{ij}\frac{v}{\sqrt{2}}. \tag{2.11}$$

Since the SM only incorporates one Higgs doublet in the potential V, the Yukawa- and mass matrices can be diagonalized simultaneously (such feature is not present in extensions of the SM in general, since extra Higgs doublets and extra Yukawa matrices appear in the Lagrangian). Although the diagonalization of the mass matrices is trivial, the Yukawa matrices remain arbitrary to some extent e.g. the Yukawa matrices contain some parameters that are not observable since they can be absorbed by redefinitions of the fermion fields.

The Yukawa sector of the SM has a high degree of freedom since there exists equivalent sets of complex Yukawa matrices $Y^{u,d}$ that will give the same mass spectra. The Yukawa couplings are therefore not uniquely defined and a conclusive fundamental explanation of their origin still does not exist. Since the Yukawa sector contains arbitrary parameters (up to the requirement that quark masses and CKM mixing are reproduced), it is not possible to interpret physics alone from them. Therefore, a more insightful study involves the parametrization of the Yukawa matrices to find correlations between the free parameters of the model and interesting flavour decays that could be smoking guns of NP.

2.4 The Cabibbo–Kobayashi–Maskawa matrix

In the SM, the essential components of $\mathcal{CP}$- and flavour-violation are introduced by the CKM matrix. Although interactions of quarks are measured with high precision, a fundamental explanation for its hierarchical structure still remains under debate. The CKM matrix has its origin in charged currents: the CKM patterns emerge when diagonalizing mass matrices and rotating quark spinors to the mass basis. Given the mass matrices in

[1] σ_2 is the second Pauli matrix.

(2.11), it is straightforward to diagonalize $M^{u,d}$ and $Y^{u,d}$ simultaneously. The physical interpretation of this is that one can transform the gauge states to the mass eigenstates while avoiding off-diagonal contributions in Yukawa matrices, that would lead to tree-level FCNC processes. Since such FCNC are only present at higher orders of perturbation theory, they must be naturally suppressed at tree-level in an extended model.

The diagonalization of the mass forms will play a major role for extensions of the theory introducing extra Higgs doublets. Motivated by this, a somewhat careful review of the transformation from the weak-eigenstate basis to the physical basis is given for fermions, focusing on basic properties of the unitary matrices $U^{u,d}_{L,R}$ that will act on $Y^{u,d}$ by performing a bi-unitary[2] transformation.

An arbitrary $n \times n$ complex matrix Y can be diagonalized by two unitary matrices U_L and U_R. Considering three fermion families and two to-be diagonalized Yukawa matrices $Y^{u,d}$, one needs four 3×3 unitary matrices $U^{u,d}_{L,R}$ to obtain the diagonal mass forms $m^{u,d}_{\text{diag}}$. In the SM, the matrices $m^{u,d}_{\text{diag}}$ are diagonal with positive entries. Then, diagonalization is achieved by performing bi-unitary transformations on the Yukawa matrices (2.11),

$$\begin{aligned} m^{u}_{\text{diag}} &= \frac{v}{\sqrt{2}} U^{u}_{L} Y^{u} U^{u\dagger}_{R} \\ m^{d}_{\text{diag}} &= \frac{v}{\sqrt{2}} U^{d}_{L} Y^{d} U^{d\dagger}_{R}. \end{aligned} \tag{2.12}$$

Bi-unitary transformations rotate a matrix by multiplying by two distinct unitary matrices, as illustrated above. Inverting these relations to express the components of $Y^{u,d}$ in terms of those of $m^{u,d}_{\text{diag}}$ and $U^{u,d}_{L,R}$, respectively, one gets

$$\begin{aligned} (Y^{u})_{ij} &= \frac{\sqrt{2}}{v} \big(U^{u\dagger}_{L} m^{u}_{\text{diag}} U^{u}_{R} \big)_{ij}, \\ (Y^{d})_{ij} &= \frac{\sqrt{2}}{v} \big(U^{d\dagger}_{L} m^{d}_{\text{diag}} U^{d}_{R} \big)_{ij}. \end{aligned} \tag{2.13}$$

To investigate the effect of these bi-unitary transformations on different sectors of the SM, we recall the Yukawa Lagrangian $\mathcal{L}_{\text{Y}}$ after SSB in (2.10) and substitute the expressions above for $Y^{u,d}$

$$\begin{aligned} -\mathcal{L}_{\text{Y}} &= \frac{v}{\sqrt{2}} Y^{d}_{i,j} \overline{d}_{Li} d_{Rj} + \frac{v}{\sqrt{2}} Y^{u}_{i,j} \overline{u}_{Li} u_{Rj} + h.c. \\ &= \big(U^{d\dagger}_{L} m^{d}_{\text{diag}} U^{d}_{R} \big)_{ij} \overline{d}_{Li} d_{Rj} + \big(U^{u\dagger}_{L} m^{u}_{\text{diag}} U^{u}_{R} \big)_{ij} \overline{u}_{Li} u_{Rj} + h.c. \\ &= (m^{d}_{\text{diag}})_{ij} \overline{d'}_{Li} d'_{Rj} + (m^{u}_{\text{diag}})_{ij} \overline{u'}_{Li} u'_{Rj} + h.c., \end{aligned} \tag{2.14}$$

where the primed fields are the fields in the mass basis. We have performed a rotation on the quark fields by means of a bi-unitary transformation and managed to express them in a basis where the mass matrix is diagonal,

$$\begin{aligned} d'_{L,R} &= U^{d}_{L,R} d_{L,R}, \\ u'_{L,R} &= U^{u}_{L,R} u_{L,R}. \end{aligned} \tag{2.15}$$

[2]This is also known as the singular value decomposition of a matrix.

The CKM matrix has its origin in the diagonalization of the mass matrices and the nature of the EW theory that includes L-handed particles and excludes R-handed ones in the $\mathrm{SU(2)_L}$ interactions. This can be explicitly seen in the EW couplings of fermions after a change of basis to the physical basis

$$\begin{aligned}\mathcal{L}_{\text{ferm}} \supset & \frac{1}{2}\overline{u}_L\gamma^\mu\big(g'Y_L B_\mu + gW^0_\mu\big)u_L - \frac{1}{\sqrt{2}}g\overline{u}_L\gamma^\mu d_L W^+_\mu \\ & - \frac{1}{\sqrt{2}}g\overline{d}_L\gamma^\mu u_L W^-_\mu + \frac{1}{2}\overline{d}_L\gamma^\mu\big(g'Y_L B_\mu - gW^0_\mu\big)d_L, \end{aligned} \tag{2.16}$$

where Y_L is the hypercharge assigned to L-handed fermions and should not be confused with the Yukawa matrices $Y^{u,d}$. Performing the inverse transformation in (2.15) to express $\mathcal{L}_{\text{ferm}}$ in terms of the quark mass eigenstates, we get

$$\begin{aligned}\mathcal{L}_{\text{ferm}} \supset & \frac{1}{2}\overline{u'}_L\gamma^\mu\big(g'Y_L B_\mu + gW^0_\mu\big)(U^u_L U^{u\dagger}_L)u'_L - \frac{1}{\sqrt{2}}g\overline{u'}_L\gamma^\mu(U^u_L U^{d\dagger}_L)d'_L W^+_\mu \\ & - \frac{1}{\sqrt{2}}g\overline{d'}_L\gamma^\mu(U^d_L U^{u\dagger}_L)u'_L W^-_\mu + \frac{1}{2}\overline{d'}_L\gamma^\mu\big(g'Y_L B_\mu - gW^0_\mu\big)(U^d_L U^{d\dagger}_L)d'_L \end{aligned} \tag{2.17}$$

Using the unitarity condition $U^{u,d}_L U^{u,d\dagger}_L = 1$ and the definition of $V_{\text{CKM}} = U^u_L U^{d\dagger}_L$ it is easy to see that interactions of fermions with neutral fields remain unchanged under the change of basis, while charged interactions are indeed sensitive to this transformation,

$$\mathcal{L}_{\text{ferm}} \supset \frac{1}{\sqrt{2}}g\overline{u'}_L\gamma^\mu V_{\text{CKM}} d'_L W^+_\mu + h.c. \tag{2.18}$$

An interesting feature of the SM is the insensitivity of interactions to the R-handed unitary matrices $U^{u,d}_R$ e.g. they are invisible to measurements: this is a consequence of the $\mathrm{SU(2)_L} \times \mathrm{U(1)_Y}$ symmetry in EW interactions, where only L-handed quarks couple and mix with each other via the CKM matrix in *charged current* interactions.

2.4.1 Physical degrees of freedom

The CKM matrix [10][11] is a 3×3 unitary matrix which can be parametrized by three mixing angles and one $\mathcal{CP}$-violating phase [11]. A matrix V is unitary if, and only if, the unitarity relations $V^\dagger V = VV^\dagger = \mathbf{1}$ are fulfilled

$$V^*_{1j}V_{1k} + V^*_{2j}V_{2k} + V^*_{3j}V_{3k} = \delta_{jk}, \tag{2.19}$$

$$V^*_{j1}V_{k1} + V^*_{j2}V_{k2} + V^*_{j3}V_{k3} = \delta_{jk}. \tag{2.20}$$

These relations can be straightforwardly derived if one recalls that the column (or row) vectors $\mathbf{a_1}, ..., \mathbf{a_n}$ of an unitary matrix $V = [\mathbf{a_1}, ..., \mathbf{a_n}]$ are orthonormal to each other, namely that $\langle \mathbf{a_i}, \mathbf{a_j} \rangle = \mathbf{a^*_i a_j} = \delta_{\mathbf{ij}}$ holds for any i,j.

The CKM matrix is naively parametrized by three mixing angles and six phases. Nevertheless, it can be shown that indeed five of these phases are not physical; they can

be absorbed into the definitions of the quark fields. On the other hand, a global phase rotation acting on all quarks, leaves the CKM unchanged. Therefore, one is left with three angles $\theta_{12}, \theta_{23}, \theta_{13}$ and one complex phase δ representing the physically relevant parameters of CKM. All freedom has been exhausted at this point. Defining the notation $\sin\theta_{ij} = s_{ij}, \cos\theta_{ij} = c_{ij}$, one can express the CKM matrix adopting the following convention

$$V_{\rm CKM} = \begin{pmatrix} c_{12}c_{13} & s_{12}c_{13} & s_{13}e^{-i\delta} \\ -(s_{12}c_{23} + c_{12}s_{23}s_{13}e^{i\delta}) & (c_{12}c_{23} - s_{12}s_{23}s_{13}e^{i\delta}) & s_{23}c_{13} \\ (s_{12}s_{23} - c_{12}c_{23}s_{13}e^{i\delta}) & -(c_{12}s_{23} + s_{12}c_{23}s_{13}e^{i\delta}) & c_{23}c_{13} \end{pmatrix}. \tag{2.21}$$

The CKM has strong hierarchies between its parameters, as suggested by the experimental data

$$s_{12} \approx 0.2, \quad s_{23} \approx 0.04, \quad s_{13} \approx 4 \times 10^{-3}, \tag{2.22}$$

which implies that CKM is rather close to unity with hierarchically small off-diagonal elements. Thus, flavour changing charged current transitions, which are proportional to the off-diagonal CKM elements, are significantly suppressed in the SM.

The parametrization of CKM used in this thesis is the one introduced by Wolfenstein [12], which explicitly parametrizes the CKM by three real and one imaginary physical parameters. The Wolfenstein parametrization is an expansion of the CKM matrix in the real parameter λ which is defined in terms of the Cabibbo angle $\lambda = \sin\theta_{12}$ as outlined in relations (2.24). Neglecting terms of order $\mathcal{O}(\lambda^4)$ we have that

$$V_{\rm CKM} = \begin{pmatrix} 1 - \frac{1}{2}\lambda^2 & \lambda & A\lambda^3(\rho - i\eta) \\ -\lambda & 1 - \frac{1}{2}\lambda^2 & A\lambda^2 \\ A\lambda^3(1 - \rho - i\eta) & -A\lambda^2 & 1 \end{pmatrix} + \mathcal{O}(\lambda^4). \tag{2.23}$$

The Wolfenstein parameters are defined in terms of three angles and the $\mathcal{CP}$-violating phase according to the following relations

$$\begin{aligned} s_{12} = \lambda = \frac{|V_{us}|}{\sqrt{|V_{ud}|^2 + |V_{us}|^2}}, \qquad s_{23} = A\lambda^2 = \lambda\Big|\frac{V_{cb}}{V_{us}}\Big|, \\ s_{13}e^{i\delta} = V_{ub}^* = A\lambda^3(\rho + i\eta) = \frac{A\lambda^3(\overline{\rho} + i\overline{\eta})\sqrt{1 - A^2\lambda^4}}{\sqrt{1-\lambda^2}[1 - A^2\lambda^4(\overline{\rho} + i\overline{\eta})]}, \end{aligned} \tag{2.24}$$

where V_{ij} for $i = u, c, t; j = d, s, b$ are the CKM elements. The fit for the Wolfenstein parameters is [9]

$$\begin{aligned} \lambda &= 0.22506 \pm 0.00050, & A &= 0.81 \pm 0.026, \\ \overline{\rho} &= 0.124^{+0.019}_{-0.018}, & \overline{\eta} &= 0.356 \pm 0.011, \end{aligned}$$

where

$$\overline{\rho} = \rho(1 - \frac{\lambda^2}{2} + ...), \quad \overline{\eta} = \eta(1 - \frac{\lambda^2}{2} + ...). \tag{2.25}$$

In this notation, $\mathcal{CP}$-violation is introduced by η and the Cabibbo angle θ_{12} is incorporated in the expansion parameter λ.

The number of physically relevant parameters can also be determined by symmetry arguments [13]. Ignoring the Yukawa sector, the SM is invariant under $G_{flavour}$, the global flavour symmetry group given by

$$G_{flavour} = \mathrm{U}(3)_{\mathrm{Q}} \times \mathrm{U}(3)_{\mathrm{U}} \times \mathrm{U}(3)_{\mathrm{D}}. \tag{2.26}$$

If the Yukawa couplings Y^u, Y^d are included in the description, the symmetry under the $G_{flavour}$ group is broken, leaving only one U(1) untouched.

At first glance, the Yukawa couplings Y^u, Y^d are arbitrary 3×3 complex matrices, contributing with a total of $18+18$ parameters. Nevertheless, not all of these are physical, in fact, each of the broken generators of the symmetry group $G_{flavour}$ corresponds to one parameter that can be absorbed by the fields. Let us notice that $\mathrm{U}(3)_{\mathrm{Q}} \times \mathrm{U}(3)_{\mathrm{U}} \times \mathrm{U}(3)_{\mathrm{D}}$ contains 9 real parameters and 18 phases. Nicely, all of these phases in Y^u, Y^d but one are not physical. The one corresponding to the unbroken U(1) remains physical. The 9 real parameters are quark masses $m_u, m_d, m_c, m_s, m_t, m_b$ and angles $\theta_{12}, \theta_{23}, \theta_{13}$. The only relevant phase is δ, the CKM phase.

The physical meaning of the phase δ in CKM is intimately related to the charge $\mathcal{C}$ and parity $\mathcal{P}$ conjugation as a combined operation. Looking at the charged current described in (2.18), it is straightforward to see that the $\mathcal{CP}$-transformation does not result in the same terms as before[3], but rather in the complex conjugate of the CKM entries. Therefore, $\mathcal{CP}$ is violated by charged currents if, and only if, $\delta \neq 0$. To finish, let us stress that δ can be shifted between the CKM elements, therefore a parametrization-invariant quantity was firstly provided by Jarlskog [14],

$$J_{\mathcal{CP}} = \mathrm{Im}(\mathrm{V_{us}V_{cb}V_{ub}^{*}V_{cs}^{*}}) \approx 3 \times 10^{-5}, \tag{2.27}$$

and quantifies the amount of $\mathcal{CP}$-violation in nature.

2.4.2 Quark mixing: Signatures of new physics

Quark mixing is extremely important for BSM physics since decays and mixings of mesons, such as B, B_s, K, and D, can help to identify particular signatures of new physics. In particular, FCNCs are processes that do not emerge at tree-level in the SM[4] but only strongly suppressed at one-loop level. In flavour-nonuniversal transitions, these flavour-violating processes are sensitive to BSM contributions and therefore, constitute sources of strong constraints on possible extensions of the SM. The BSM contributions of neutral mesons decays, for example

$$\begin{aligned} \overline{B} &\to X_s\gamma, X_s\overline{\ell}\ell, \overline{\ell}\ell \\ K^+ &\to \pi^+\nu\overline{\nu}, \end{aligned} \tag{2.28}$$

[3]This is not the case of the neutral current where mediators are Z^0, γ, g. This is indeed a $\mathcal{CP}$-invariant transition.

[4]Due to diagonal Yukawa matrices in the mass basis.

are suppressed by powers of the energy scale of the NP contributions. Particularly interesting for us, is the scenario where FCNCs appear not only at loop-level but also at tree-level in the Lagrangian. Such tree-level FCNCs can emerge, for example, in theories with extended Higgs sectors as a result of non-diagonal structures of the Yukawa matrices $Y^{u,d}$. Such extended models need to agree with the current constraints from measurements which are close to the SM predictions. Therefore, in such extended models, a mechanism of tree-level FCNC-suppression is needed, typically, by almost vanishing Yukawa couplings or a large mass scale of non-standard scalar states.

2.5 Flavour Changing Neutral Currents in the SM

We have seen in (2.18) that charged currents mediate transitions that change *flavour*: they occur at tree-level in the SM with the strength of the interactions ruled by CKM off-diagonal terms. On the contrary, FCNCs in the SM are not present at tree-level: the couplings of neutral current interactions are flavour-diagonal. FCNCs in the SM take place only at loop-level with internal $W^{\pm}$ boson e.g. in neutral B_s meson mixing. The amplitude of one of the Feynman diagrams contributing to this process (see figure 1) scales as [13],

$$\mathcal{M} \propto \sum_{i,j=u,c,t} V_{is}^* V_{ib} V_{js}^* V_{jb}^* F(x_i, x_j) \tag{2.29}$$

where the function $F(x_i, x_j)$ is the loop function with $x_i = (m_i/M_W)^2$, being m_i the i-th up-type quark mass. Using the unitarity relations $\sum_{i=u,c,t} V_{is}^* V_{ib}$ from CKM, assuming small up and charm quark mass $m_u, m_c \approx 0$ and the flavour-hierarchy $V_{cb}^* V_{cb} \ll V_{tb}^* V_{tb}$, the amplitude takes the form,

$$\mathcal{M} \propto (V_{ts}^* V_{tb})^2 S_0(x_t) \tag{2.30}$$

where $S_0(x_t) = F(x_t, x_t) - 2F(0, x_t) + F(0, 0)$. Indeed, the smallness of this FCNC is controlled by a small V_{ts} and a loop suppression factor. The Glashow–Iliopoulos–Maiani mechanism (GIM) provides an additional suppression [15]: quark terms that do not depend on mass are cancelled in the loop by the CKM unitarity and only differences of mass dependent ones contribute.

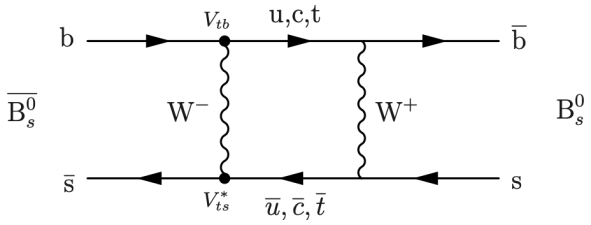

Figure 1: One-loop Feynman diagram contributing to the $\overline{B}_s^0 - B_s^0$ transition in the SM.

2.5.1 Rare K decays

Rare and $\mathcal{CP}$-violating K decays such as $K_L \to \pi^0\nu\overline{\nu}$ (see figure 2) can deliver interesting signatures of NP [16]. These type of decays, which generate FCNCs mediated at quark level by the transition $s \to d$, have a strong suppression in the SM due to the flavour hierarchy of CKM and the GIM mechanism. Therefore, large NP contributions are realizable even if the NP energy scale is well above the TeV scale [13]. We focus our attention on the kaon decays $K^+ \to \pi^+\nu\overline{\nu}$ and $K_L \to \pi^0\nu\overline{\nu}$ since they are very well predicted by theory and dramatically suppressed in the SM. Thus, these decays are remarkably sensitive to NP [17].

The $K^+ \to \pi^+\nu\overline{\nu}$ decays are mediated in the SM by the neutral Z gauge boson in the Z-penguin and box diagrams (see figure 2). The complete form of the effective Hamiltonian $\mathcal{H}_{eff}$ is important since it presents the different terms contributing to the $K^+ \to \pi^+\nu\overline{\nu}$ transition including next-to-leading order corrections. The first term in $\mathcal{H}_{eff}$ in (2.31) is the charm quark contribution known to next-to-next-to-leading order (NNLO) in QCD and next-to-leading order (NLO) in EW theory and it is only important to the $\mathcal{CP}$-preserving decay $K^+ \to \pi^+\nu\overline{\nu}$. The second term is the top quark loop contribution and affects both the $\mathcal{CP}$-preserving mode $K^+ \to \pi^+\nu\overline{\nu}$ and the $\mathcal{CP}$-violating mode $K_L \to \pi^0\nu\overline{\nu}$. The explicit form of the $\mathcal{H}_{eff}$ describing the K decays is given by [18]

$$\mathcal{H}_{eff} = \frac{G_F}{\sqrt{2}}\frac{\alpha}{2\pi\sin^2\theta_W}\sum_{\ell=e,\mu,\tau}\left(V_{cs}^*V_{cd}X_{NL}^{\ell}(x_c) + V_{ts}^*V_{td}X(x_t)\right)(\overline{s}d)_{V-A}(\overline{\nu}_\ell\nu_\ell)_{V-A}, \quad (2.31)$$

where the factors X^ℓ are the Wilson coefficients of a given lepton ℓ, α is the weak coupling at a given energy scale, G_F is the Fermi constant, θ_W is the Weinberg angle, and the subscript NL refers to next-to-leading order of perturbation theory. The charged lepton mass dependence that arises from the box diagram, is negligible for the top quark contribution. For the charm quark, this is only the case for e and μ and not for the τ lepton. The function $X(x)$ in (2.31) is given by

$$X(x) = X_0(x) + \frac{\alpha_s}{4\pi}X_1(x). \quad (2.32)$$

Here, α_s is the strong coupling and we have defined the argument of (2.32) as $x_i = m_i^2/M_W^2$ (for $i = c, t$). Moreover, $X_0(x)$ and $X_1(x)$ are QCD correction functions which we have defined in Appendix C.

NP contributions to the Hamiltonian in (2.31) can be parametrized[5] by doing the replacement $X(x_t) \to X$ where [19]

$$X = |X|e^{i\theta_X}. \quad (2.33)$$

Therefore, measuring $\mathcal{BR}(K^+ \to \pi^+\nu\overline{\nu})$ and $\mathcal{BR}(K_L \to \pi^0\nu\overline{\nu})$ determines both θ_X and $|X|$ and any deviations from $\theta_X = 0$[6] and $|X| = X(x_t)$, is a smoking-gun for NP.

[5] This parametrization is model-independent.

[6] This phase is forced to take the values $\theta_X \approx 0, \frac{\pi}{2}, \pi, \frac{3\pi}{2}$.

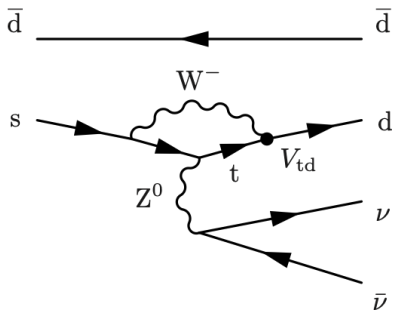

Figure 2: Penguin Feynman diagram of the process $\overline{K^0} \to \pi^0 \nu\overline{\nu}$.

2.5.2 B meson physics

After the ever first detection of the $B_d - \overline{B}_d$ oscillations with the ARGUS detector [20], B meson physics has become an attractive playground to determine with high accuracy the CKM elements $|V_{ub}|$, $|V_{cb}|$ and the amount of $\mathcal{CP}$-violation in the $B_d - \overline{B}_d$ system [21][22]. Observations of oscillations in the $B_s - \overline{B}_s$ system were again later detected at FERMILAB [23] and confirmed at LHCb [24]. In this subsection, we briefly describe some of the decays of the B mesons (see e.g. figure 3), which can deliver signatures of NP as discussed in section 2.4.2.

In order to describe the decays $B_{d,s} \to \overline{\mu}\mu$ and some other decays governed by the transition $b \to s\bar{\ell}\ell$, such as $B \to K^*\bar{\ell}\ell$, $B \to K\bar{\ell}\ell$ and $B \to X_s\bar{\ell}\ell$, we need the corresponding effective Hamiltonian $\mathcal{H}_{eff}(b \to s\bar{\ell}\ell)$, which is given by [25]

$$\begin{aligned}\mathcal{H}_{eff}(b \to s\bar{\ell}\ell) &= \mathcal{H}_{eff}(b \to s\gamma) \\ &\quad - \frac{4G_F}{\sqrt{2}}\frac{\alpha}{4\pi}V_{ts}^*V_{tb}\sum_{i=9,10,S,P}\Big[C_i(\mu)Q_i(\mu) + C_i'(\mu)Q_i'(\mu)\Big],\end{aligned} \tag{2.34}$$

where the operators $Q_{9,10,S,P}^{(\prime)}$ in front of the Wilson coefficients $C_{9,10,S,P}^{(\prime)}$ are given by

$$\begin{aligned} Q_9 &= (\bar{s}\gamma_\mu P_L b)(\bar{\ell}\gamma^\mu \ell), & Q_9' &= (\bar{s}\gamma_\mu P_R b)(\bar{\ell}\gamma^\mu \ell), \\ Q_{10} &= (\bar{s}\gamma_\mu P_L b)(\bar{\ell}\gamma^\mu\gamma_5 \ell), & Q_{10}' &= (\bar{s}\gamma_\mu P_R b)(\bar{\ell}\gamma^\mu\gamma_5 \ell), \\ Q_S &= m_b(\bar{s}P_R b)(\bar{\ell}\ell), & Q_S' &= m_b(\bar{s}P_L b)(\bar{\ell}\ell), \\ Q_P &= m_b(\bar{s}P_R b)(\bar{\ell}\gamma_5 \ell), & Q_P' &= m_b(\bar{s}P_L b)(\bar{\ell}\gamma_5 \ell). \end{aligned} \tag{2.35}$$

The factor m_b in the definition of the scalar operators enforces that their matrix elements and their Wilson coefficients are not dependent of the energy scale. The $\mathcal{H}_{eff}(b \to s\gamma)$ in (2.34) is the effective Hamiltonian for the transition $b \to s\gamma$, which is described by the

dipole operators given by [26]

$$
\begin{aligned}
Q_7 &= \frac{e}{16\pi^2} m_b \overline{s}_{L,\alpha} \sigma^{\mu\nu} b_{R,\alpha} F_{\mu\nu}, \\
Q_7' &= \frac{e}{16\pi^2} m_b \overline{s}_{R,\alpha} \sigma^{\mu\nu} b_{L,\alpha} F_{\mu\nu}, \\
Q_8 &= \frac{g_s}{16\pi^2} m_b \overline{s}_{L,\alpha} \Big(\frac{\lambda^a}{2}\Big)_{\alpha,\beta} \sigma^{\mu\nu} b_{R,\beta} G^a_{\mu\nu}, \\
Q_8' &= \frac{g_s}{16\pi^2} m_b \overline{s}_{R,\alpha} \Big(\frac{\lambda^a}{2}\Big)_{\alpha,\beta} \sigma^{\mu\nu} b_{L,\beta} G^a_{\mu\nu}.
\end{aligned} \tag{2.36}
$$

The operators $Q^{(\prime)}_{7,8}$ above are computed at the energy scale μ_b. Here, the tensors $F_{\mu\nu}$ and $G^a_{\mu\nu}$ correspond to the electromagnetic and gluon field strength tensors, respectively. Furthermore, the matrices $\lambda^a, a = 1, ..., 8$ are the well-known Gell-Mann matrices and the tensor $\sigma^{\mu\nu}$ is defined in terms of the gamma matrices $\sigma^{\mu\nu} = \frac{i}{2}[\gamma^\mu, \gamma^\nu]$.

The Wilson coefficients C_9 and C_{10} in (2.34) do not have NP contributions coming from non-SM scalars exchanges and assume SM values, namely [25]

$$\sin^2\theta_W C_9^{SM} = [\eta_Y Y_0(x_t) - 4\sin^2\theta_W Z_0(x_t)], \tag{2.37}$$

$$\sin^2\theta_W C_{10}^{SM} = -\eta_Y Y_0(x_t), \tag{2.38}$$

where the functions $Y_0(x_t)$ and $Z_0(x_t)$ are SM one-loop functions given in Appendix D. The factor η_Y is a QCD factor that with $m_t = m_t(m_t)$ assumes a value very close to unity, namely $\eta_Y = 1.012$ [27][28].

For the Wilson coefficients of the scalar operators one has that [25]

$$
\begin{aligned}
m_b(\mu_H)\sin^2\theta_W C_S &= \frac{1}{g^2_{SM}} \frac{1}{M_H^2} \frac{\Delta_R^{sb}(H)\Delta_S^{\mu\overline{\mu}}(H)}{V_{ts}^* V_{tb}}, \\
m_b(\mu_H)\sin^2\theta_W C_S' &= \frac{1}{g^2_{SM}} \frac{1}{M_H^2} \frac{\Delta_L^{sb}(H)\Delta_S^{\mu\overline{\mu}}(H)}{V_{ts}^* V_{tb}}, \\
m_b(\mu_H)\sin^2\theta_W C_P &= \frac{1}{g^2_{SM}} \frac{1}{M_H^2} \frac{\Delta_R^{sb}(H)\Delta_P^{\mu\overline{\mu}}(H)}{V_{ts}^* V_{tb}}, \\
m_b(\mu_H)\sin^2\theta_W C_P' &= \frac{1}{g^2_{SM}} \frac{1}{M_H^2} \frac{\Delta_L^{sb}(H)\Delta_P^{\mu\overline{\mu}}(H)}{V_{ts}^* V_{tb}},
\end{aligned} \tag{2.39}
$$

where H is a neutral mass eigenstate with mass M_H. Furthermore, we have introduced the definition of g^2_{SM}

$$g^2_{SM} = 4\frac{G_F}{\sqrt{2}} \frac{\alpha}{2\pi\sin^2\theta_W}, \tag{2.40}$$

and the scalar and pseudo-scalar couplings of H to $\mu\overline{\mu}$, namely $\Delta_S^{\mu\overline{\mu}}(H)$ and $\Delta_P^{\mu\overline{\mu}}(H)$, respectively [25]:

$$\Delta_S^{\mu\overline{\mu}}(H) = \Delta_R^{\mu\overline{\mu}}(H) + \Delta_L^{\mu\overline{\mu}}(H), \tag{2.41}$$

$$\Delta_P^{\mu\overline{\mu}}(H) = \Delta_R^{\mu\overline{\mu}}(H) - \Delta_L^{\mu\overline{\mu}}(H). \tag{2.42}$$

Moreover, the couplings of neutral scalars H to quarks are denoted by $\Delta^{ij}_{L,R}(H)$, where the indices i, j denote the quark flavour. Therefore, transitions such as $b \to s\bar{\ell}\ell$ are governed by $\Delta^{ij}_{L,R}(H)$ with the property that $\Delta^{ij}_{L}(H) = [\Delta^{ji}_{R}(H)]^*$.

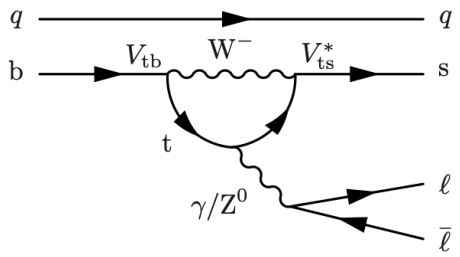

Figure 3: Virtual Z^0/γ in the penguin diagram of the transition $b \to s\ell\bar{\ell}$. The transition $b \to s\gamma$ is also described by this penguin diagram where γ is on mass-shell.

3 $\mathrm{U}(1) \times \mathrm{Z}_2$ Flavoured 3HDM

Extensions of the SM with three Higgs doublets open the door to some of the unexplored characteristics of the SM while providing rich and still tractable phenomenology. It is aesthetically appealing to imagine that three families of Higgs scalars and three families of fermions are maybe realized in nature. Motivated by this idea, one could ask what would happen if a *flavour symmetry* is introduced to a 3HDM in such a way that the model is phenomenologically consistent with experiments.

General Three Higgs Doublet Models without any imposed symmetries suffer from FCNCs at tree-level. One way of preventing the appearance of such tree-level FCNCs is through the implementation of a discrete symmetry that leads to natural flavour conservation (NFC) [26]. Another way of avoiding FCNCs at tree-level is by having Yukawa matrices that are proportional to each other. An interesting way of securing NFC is done in Branco, Grimus and Lavoura (BGL) models [29], where tree-level FCNCs are naturally suppressed by an exact symmetry of the Lagrangian being broken by the neutral Higgs fields VEVs.

Our 3HDM is a new model, currently not present in the literature. This thesis studies the main features and the phenomenological consistency of such a 3HDM for the first time. Also, this project represents a natural continuation of the work done by the authors in [5], who studied a 3HDM model with a $\mathrm{U}(1) \times \mathrm{U}(1)$ symmetry. Despite the similarities between the model in [5] and ours, there are some important differences between both models; they have assumed a hierarchy in the VEVs $v_1, v_2 \ll v_3$, while we do not take this limit but allow v_1, v_2, v_3 to move freely across their domain. Also, the aforementioned model did not include tree-level FCNCs, where the CKM matrix was not reproduced but only Cabibbo mixing was incorporated. Once again, in this thesis, we would like to resolve this last drawback and offer a more realistic model capable of reproducing the SM flavour structure, as discussed in depth in the results section 4.2.

The model is a 3HDM with a $\mathrm{U}(1) \times \mathrm{Z}_2$ global symmetry in the scalar- and fermion sector. This $\mathrm{U}(1) \times \mathrm{Z}_2$ symmetry constrains the terms that can appear in the flavour sector of the Lagrangian resulting in very specific structures (or textures) of the Yukawa couplings. Due to the presence of three Higgs doublets in our model, larger symmetries can be imposed in our extended potential since one has the freedom to assign charges to the fields in different ways. By determining the $U(1) \times \mathrm{Z}_2$ charges to the doublets and singlets one determines how they transform under this symmetry. Let us mention that this model does not introduce extra sources of $\mathcal{CP}$-violation apart from the one provided in the SM, as discussed in section 2.2.

We adopt the following field content

$$\begin{aligned} Q_{L,i} = \begin{pmatrix} u_{L,i} \\ d_{L,i} \end{pmatrix}, \qquad \Psi_{L,i} = \begin{pmatrix} \nu_{L,i} \\ e_{L,i} \end{pmatrix}, \\ u_{R,i}, \quad d_{R,i}, \quad e_{R,i}, \quad i = 1,2,3, \\ H_j = \begin{pmatrix} H_j^+ \\ \frac{1}{\sqrt{2}}(\phi_j + i\sigma_j + v_j) \end{pmatrix}, \quad j = 1,2,3, \end{aligned} \tag{3.1}$$

where $Q_{L,i}, H_j, \Psi_{L,i}$ and $u_{R,i}, d_{R,i}, e_{R,i}$ are $\mathrm{SU}(2)_\mathrm{L}$ doublets and singlets of the i-th and j-th generation, respectively. Here H_j^+, ϕ_j, and σ_j are the charged-, $\mathcal{CP}$-even and $\mathcal{CP}$-odd Higgs fields. The j-th Higgs doublet H_j acquires the VEV v_j after SSB, which is assumed to be real for all $j = 1,2,3$. Thus, no spontaneous $\mathcal{CP}$-violation is included here.

The choice for the charges is motivated by having the $U(1) \times \mathrm{Z}_2$ symmetry softly broken, which will help avoiding the appearance of a massless Goldstone state. Also, in the fermion sector, this leads to particular textures for the Yukawa matrices needed to reproduce the flavour structure in the SM. The assigned charges are the following

$$\begin{aligned} U(1): \quad & Q_{L,3} \to e^{i\alpha} Q_{L,3} & \mathrm{Z}_2: \quad & \mathrm{Q}_{\mathrm{L},3} \to -Q_{L,3} \\ & u_{R,3} \to e^{2i\alpha} u_{R,3} & & u_{R,3} \to -u_{R,3} \\ & H_1 \to e^{i\alpha} H_1 & & H_1 \to -H_1 \\ & \Psi_{L,i} \to e^{i\alpha} \Psi_{L,i} & & \Psi_{L,i} \to -\Psi_{L,i} \\ & H_3 \to e^{i\alpha} H_3 & & d_{R,3} \to -d_{R,3} \end{aligned} \tag{3.2}$$

The other fields remain unchanged under the imposed $U(1) \times \mathrm{Z}_2$ global symmetry. This set of transformations will constrain specific structures for the Yukawa matrices in the fermion sector of the model, as well as the type of $\mathrm{SU}(2)_\mathrm{L}$ doublets H_i couplings that can stand in the scalar potential V. These transformations completely determine both the scalar- and fermionic sector of our 3HDM.

3.1 Yukawa sector

Let us consider the Yukawa sector invariant under the $U(1) \times \mathrm{Z}_2$ symmetry. The Yukawa Lagrangian has been defined in terms of three up-type and three down-type complex Yukawa

matrices and one real lepton Yukawa matrix. The quark sector of the Yukawa potential is shown in its most general form while the lepton sector follows a specific choice of our model, as shown here

$$\begin{aligned}-\mathcal{L}_Y = \sum_{a,b=1}^{3} \Big\{ & \overline{Q}_{La}(Y_1^d)_{ab} H_1 d_{Rb} + \overline{Q}_{La}(Y_2^d)_{ab} H_2 d_{Rb} + \overline{Q}_{La}(Y_3^d)_{ab} H_3 d_{Rb} \\ & - \overline{Q}_{La}(Y_1^u)_{ab}(\epsilon H_1^*) u_{Rb} - \overline{Q}_{La}(Y_2^u)_{ab}(\epsilon H_2^*) u_{Rb} - \overline{Q}_{La}(Y_3^u)_{ab}(\epsilon H_3^*) u_{Rb} \\ & + \overline{\Psi}_{La}(Y_1^e)_{ab} H_1 e_{Rb} + h.c. \Big\}. \end{aligned} \tag{3.3}$$

The minus sign in front of down-type couplings is needed so our definitions match the convention in `SARAH` [30]. This does not affect the physics in any way because such a minus sign can always be absorbed in the definition of the fields.

In this model, the lepton Yukawa matrix is assumed to be diagonal as in the SM, allowing leptons to couple exclusively to the lightest doublet H_1. The real lepton Yukawa matrix is

$$Y_1^e = \frac{\sqrt{2}}{v_1} \begin{pmatrix} m_e & 0 & 0 \\ 0 & m_\mu & 0 \\ 0 & 0 & m_\tau \end{pmatrix}. \tag{3.4}$$

Since there is a proportionality relation between the mass matrix m_e and the leptonic Yukawa matrix Y_1^e, FCNCs at tree-level will not be mediated by leptons here. The mass matrix for leptons in the gauge basis (e_L, e_R^*) has the following form

$$m_e = \frac{1}{\sqrt{2}} v_1 Y_1^e. \tag{3.5}$$

Let us further discuss the fermion Lagrangian by studying the quark sector of our model in what follows. The quark Yukawa matrices must adopt the following textures by requiring the invariance of the Yukawa Lagrangian with respect to the family symmetry transformations given in (3.2),

$$Y_1^d = \begin{pmatrix} 0 & 0 & 0 \\ 0 & 0 & 0 \\ \times & \times & 0 \end{pmatrix}; \quad Y_1^u = \begin{pmatrix} 0 & 0 & 0 \\ 0 & 0 & 0 \\ 0 & 0 & 0 \end{pmatrix}; \tag{3.6}$$

$$Y_2^d, Y_2^u = \begin{pmatrix} \times & \times & 0 \\ \times & \times & 0 \\ 0 & 0 & 0 \end{pmatrix}; \quad Y_3^d, Y_3^u = \begin{pmatrix} 0 & 0 & 0 \\ 0 & 0 & 0 \\ 0 & 0 & \times \end{pmatrix}, \tag{3.7}$$

where the $\times$ refers to an arbitrary complex entry. One can check that this set of Yukawa matrices prevent the $\mathcal{L}_Y$ to have terms that are not invariant under the imposed family symmetries. The textures of the Yukawa matrices and the size of their components will determine the strength of FCNCs at tree- and loop-levels.

A set of Yukawa matrices $Y_1^d, Y_2^d, Y_3^d, Y_1^u, Y_2^u, Y_3^u$ that results in FCNCs that are controlled by the off-diagonal CKM matrix elements are given in (3.7), following the same approach that BGL models implement. We will show in the next section that some tree-level FCNCs can be indeed suppressed using the textures in (3.7), which is an important feature of our model. The imposed family symmetry transformations in (3.2) result in FCNCs in the down sector, mediated by the heavy neutral scalars H_2, H_3, which are the mass eigenstates of ϕ_1, ϕ_2 and ϕ_3. Let us focus on the coupling of quarks to the scalar-, pseudo-scalar and charged Higgs fields to gain insight into the phenomenology of the 3HDM model. Let us express $\mathcal{L}_{\rm Y}$ after SSB where the scalar fields acquire VEVs and study the couplings of the scalar fields with quarks

$$\begin{aligned}
-\mathcal{L}_{\rm Y} &= \sum_{i=1}^{3} \Big\{ \left(\overline{u}_{La} \quad \overline{d}_{La}\right) (Y_i^d)_{ab} \begin{pmatrix} H_i^+ \\ \frac{\phi_i + i\sigma_i}{\sqrt{2}} \end{pmatrix} d_{Rb} \\
&\quad - \left(\overline{u}_{La} \quad \overline{d}_{La}\right) (Y_i^u)_{ab} i\sigma_2 \begin{pmatrix} H_i^- \\ \frac{\phi_i - i\sigma_i}{\sqrt{2}} \end{pmatrix} u_{Rb} + h.c. \Big\} \\
&= \sum_{i=1}^{3} \Big\{ (Y_i^d)_{ab} \Big[\overline{u}_{La} H_i^+ + \frac{1}{\sqrt{2}} \overline{d}_{La} (\phi_i + i\sigma_i) \Big] d_{Rb} \\
&\quad - (Y_i^u)_{ab} \Big[\frac{1}{\sqrt{2}} \overline{u}_{La} (\phi_i - i\sigma_i) - \overline{d}_{La} H_i^- \Big] u_{Rb} + h.c. \Big\}. \qquad (3.8)
\end{aligned}$$

Let us assume the following parametrization of the VEVs $v_1 = v\cos\psi_2 \sin\psi_1$, $v_2 = v\sin\psi_2$, $v_3 = v\cos\psi_1\cos\psi_2$ where $\sqrt{v_1^2 + v_2^2 + v_3^2} \approx 246$ GeV holds for arbitrary ψ_1, ψ_2. Defining the rotation $\mathcal{O}_{\psi_1\psi_2}$ which brings us to the Higgs basis where the mass matrices $m^2_{A^0}$ and $m^2_{H^\pm}$ are block-diagonal, one can express $\mathcal{L}_{\rm Y}$ in terms of the physical Higgs fields. Let us define the following orthogonal matrix $\mathcal{O}_{\psi_1\psi_2}$,

$$\mathcal{O}_{\psi_1\psi_2} = \begin{pmatrix} \frac{v_1}{v} & \frac{v_2}{v} & \frac{v_3}{v} \\ \frac{v_3}{v_{13}} & 0 & -\frac{v_1}{v_{13}} \\ \frac{v_1 v_2}{v v_{13}} & -\frac{v_{13}}{v} & \frac{v_2 v_3}{v v_{13}} \end{pmatrix} = \begin{pmatrix} \cos\psi_2 \sin\psi_1 & \sin\psi_2 & \cos\psi_2\cos\psi_1 \\ \cos\psi_1 & 0 & -\sin\psi_1 \\ \sin\psi_1\sin\psi_2 & -\cos\psi_2 & \cos\psi_1\sin\psi_2 \end{pmatrix}, \qquad (3.9)$$

where $v_{13} = \sqrt{v_1^2 + v_3^2}$. Then, the basis transformation reads as,

$$\begin{pmatrix} \phi_1 \\ \phi_2 \\ \phi_3 \end{pmatrix} = \mathcal{O}^T_{\psi_1\psi_2} \begin{pmatrix} h_1 \\ h_2 \\ h_3 \end{pmatrix}, \qquad (3.10)$$

$$\begin{pmatrix} H_1^\pm \\ H_2^\pm \\ H_3^\pm \end{pmatrix} = \mathcal{O}^T_{\psi_1\psi_2} \begin{pmatrix} \omega^\pm \\ H_1^{\pm\prime} \\ H_2^{\pm\prime} \end{pmatrix}, \qquad (3.11)$$

$$\begin{pmatrix} \sigma_1 \\ \sigma_2 \\ \sigma_3 \end{pmatrix} = \mathcal{O}^T_{\psi_1\psi_2} \begin{pmatrix} \xi \\ A_1^0 \\ A_2^0 \end{pmatrix}, \qquad (3.12)$$

where h_i are the neutral scalar states, $H^{\pm\prime}_{1,2}$ charged scalar states and $A^0_{1,2}$ neutral pseudo-scalar states in the Higgs basis. In this intermediate basis, the presence of the massless Goldstone bosons $\omega^\pm$ and ξ is explicit, which then become the longitudinal polarizations of the weak bosons $W^\pm$ and Z, respectively. Expanding the summation and implementing the Yukawa textures of our model, the couplings of the various scalars with the fermions become explicit. For example, the coupling of the scalars with up-quarks and down-quarks is

$$-\mathcal{L}_{\rm Y} = \overline{u}_{La} d_{Rb} \Bigg\{ Y^d_{1ab}\Big(\frac{v_1}{v}\omega^+ + \frac{v_3}{v_{13}}H_1^{+\prime} + \frac{v_1 v_2}{v v_{13}}H_2^{+\prime}\Big) + Y^d_{2ab}\Big(\frac{v_2}{v}\omega^+ - \frac{v_{13}}{v}H_2^{+\prime}\Big) + Y^d_{3ab}\Big(\frac{v_3}{v}\omega^+ - \frac{v_1}{v_3}H_1^{+\prime} + \frac{v_2 v_3}{v v_{13}}H_2^{+\prime}\Big)\Bigg\}. \tag{3.13}$$

Once all Yukawa couplings are known, one can ask whether FCNC appear at tree-level in the model and whether they have a substantial contribution compared to the corresponding SM processes. To investigate FCNCs, one attempts to diagonalize the up-type and down-type mass matrices that are generated after SSB. To this end, let the Higgs fields acquire VEV and generate quark masses via the Higgs mechanism,

$$\begin{aligned} -\mathcal{L}_{\rm Y} &= \sum_{i=1}^{3} \Big\{ \begin{pmatrix}\overline{u}_{La} & \overline{d}_{La}\end{pmatrix} (Y^d_i)_{ab} \begin{pmatrix} 0 \\ \frac{v_i}{\sqrt{2}} \end{pmatrix} d_{Rb} - \begin{pmatrix}\overline{u}_{La} & \overline{d}_{La}\end{pmatrix} (Y^u_i)_{ab} \begin{pmatrix} \frac{v_i}{\sqrt{2}} \\ 0 \end{pmatrix} u_{Rb} + h.c. \Big\} \\ &= \sum_{i=1}^{3} \Big\{ \frac{v_i}{\sqrt{2}} (Y^d_i)_{ab} \overline{d}_{La} d_{Rb} - \frac{v_i}{\sqrt{2}} (Y^u_i)_{ab} \overline{u}_{La} u_{Rb} + h.c. \Big\} \end{aligned} \tag{3.14}$$

The mass matrices can be identified after SSB as the coefficients in front of the quark bi-linears

$$(m^d)_{ab} = \frac{v_1}{\sqrt{2}}(Y^d_1)_{ab} + \frac{v_2}{\sqrt{2}}(Y^d_2)_{ab} + \frac{v_3}{\sqrt{2}}(Y^d_3)_{ab} \tag{3.15}$$

$$(m^u)_{ab} = \frac{v_1}{\sqrt{2}}(Y^u_1)_{ab} + \frac{v_2}{\sqrt{2}}(Y^u_2)_{ab} + \frac{v_3}{\sqrt{2}}(Y^u_3)_{ab} \tag{3.16}$$

In the SM, the diagonalization of the Yukawa matrices follows automatically after diagonalizing the mass matrices (see equation 2.11). In the 3HDM scenario, this is not true in general since now the mass matrix is composed by two additional matrices with more general structures, which induce tree-level FCNCs. Given the textures in (3.7) the mass matrices have the following structure

$$m^u = \begin{pmatrix} \times & \times & 0 \\ \times & \times & 0 \\ 0 & 0 & \times \end{pmatrix}, \quad m^d = \begin{pmatrix} \times & \times & 0 \\ \times & \times & 0 \\ \times & \times & \times \end{pmatrix}. \tag{3.17}$$

we now attempt to diagonalize the mass matrix m^u by means of two general 3×3 unitary matrices U^u_L, U^u_R similarly as we did in the SM case

$$m^u_{\text{diag}} = U^u_L\Big(\frac{v_1}{\sqrt{2}}Y^u_1 + \frac{v_2}{\sqrt{2}}Y^u_2 + \frac{v_3}{\sqrt{2}}Y^u_3\Big)U^{u\dagger}_R \sim U^u_L \begin{pmatrix} \times & \times & 0 \\ \times & \times & 0 \\ 0 & 0 & \times \end{pmatrix} U^{u\dagger}_R. \tag{3.18}$$

Since Y^u_1, Y^u_3 already have diagonal structure, it suffices to diagonalize Y^u_2 to obtain a diagonal mass matrix. Furthermore, given that Y^u_2 is block diagonal and has non-vanishing elements $(Y^u_2)_{ab}$ for $a, b = 1, 2$, the matrices $U^u_{L,R}$ must adopt the following textures,

$$U^u_L = \begin{pmatrix} \times & \times & 0 \\ \times & \times & 0 \\ 0 & 0 & 1 \end{pmatrix}, \qquad U^u_R = \begin{pmatrix} \times & \times & 0 \\ \times & \times & 0 \\ 0 & 0 & e^{ia} \end{pmatrix}, \tag{3.19}$$

where a phase a can be introduced into the matrix U^u_R. The unitary matrices U^u_L, U^u_R can be parametrized by two angles χ_1, χ_2, respectively. For the case of down-type quarks, the structure of these matrices is more general since Y^d_1 introduces off-diagonal terms.

$$m^d_{\text{diag}} = U^d_L\Big(\frac{v_1}{\sqrt{2}}Y^d_1 + \frac{v_2}{\sqrt{2}}Y^d_2 + \frac{v_3}{\sqrt{2}}Y^d_3\Big)U^{d\dagger}_R \sim U^d_L \begin{pmatrix} \times & \times & 0 \\ \times & \times & 0 \\ \times & \times & \times \end{pmatrix} U^{d\dagger}_R, \tag{3.20}$$

where one pair of suitable unitary matrices with the following general structure are needed to diagonalize m^d,

$$U^d_L, U^d_R = \begin{pmatrix} \times & \times & \times \\ \times & \times & \times \\ \times & \times & \times \end{pmatrix}. \tag{3.21}$$

In general one needs three angles to parametrize a 3×3 unitary U^d_L matrix. Nevertheless, one angle χ_3 is enough to parametrize both U^d_L, U^d_R matrices, since they are related by the CKM matrix and the textures (3.7) fix the remaining two angles. Now that the textures of the matrices $U^{u,d}_{L,R}$ have been found, one can ask what is the dependence of tree-level FCNCs on this set of matrices $U^{u,d}_{L,R}$.

3.2 Tree-level Flavour Changing Neutral Currents

Let us first study the couplings of down-type quarks with the neutral scalar h_2, namely

$$\mathcal{L}_{\text{Y}} \supset \frac{1}{\sqrt{2}}\bar{d}_{La}d_{Rb}\Big[Y^d_{1ab}\frac{v_3}{v_{13}} - Y^d_{3ab}\frac{v_1}{v_{13}}\Big]h_2 + h.c. \tag{3.22}$$

In order study the down-type couplings with Higgs doublets, it comes in handy to find relations between the down type Yukawa matrices Y^d_i and the diagonal mass matrix m^d,

while showing what role the CKM matrix plays in the suppression of tree-level FCNCs. Let us recall the definition of the CKM matrix

$$V_{\text{CKM}} = U_L^u U_L^{d\dagger}. \tag{3.23}$$

As shown in relations 3.19, it is straightforward to see that the following equality most hold

$$\Rightarrow \begin{pmatrix} V_{ud} & V_{us} & V_{ub} \\ V_{cd} & V_{cs} & V_{cb} \\ V_{td} & V_{ts} & V_{tb} \end{pmatrix} = \begin{pmatrix} U^u_{L,11} & U^u_{L,12} & 0 \\ U^u_{L,21} & U^u_{L,22} & 0 \\ 0 & 0 & e^{ia} \end{pmatrix} \begin{pmatrix} U^d_{L,11} & U^d_{L,12} & U^d_{L,13} \\ U^d_{L,21} & U^d_{L,22} & U^d_{L,23} \\ U^d_{L,31} & U^d_{L,32} & U^d_{L,33} \end{pmatrix}^\dagger,$$

where the elements of the last row of U_L^d are completely determined by the elements V_{ti} $(i = d, s, b)$ of the CKM matrix up to a phase,

$$V_{tj} = e^{ia}(U_L^{d*})_{j3}, \quad j = d, s, b. \tag{3.24}$$

Motivated by the block-diagonal structure of U_L^u, we define the projection operator P which extracts the elements of the last row of a matrix

$$P = \begin{pmatrix} 0 & 0 & 0 \\ 0 & 0 & 0 \\ 0 & 0 & 1 \end{pmatrix}, \qquad (P)_{ab} = \delta_{3a}\delta_{3b}. \tag{3.25}$$

By applying the operator P to the mass matrices $m^{u,d}$ one can isolate the off-diagonal terms that spoil the block-diagonal structure. One can easily verify that the following relations hold for P as in (3.25) and Y_i^d as in (3.7)

$$\begin{aligned} Pm^d &= \frac{v_1}{\sqrt{2}} Y_1^d + \frac{v_3}{\sqrt{2}} Y_3^d \\ \Rightarrow Y_1^d &= \frac{\sqrt{2}}{v_1} Pm^d - \frac{v_3}{v_1} Y_3^d, && (3.26) \\ Pm^u &= \frac{v_3}{\sqrt{2}} Y_3^d, && (3.27) \\ m_d - Pm_d &= \frac{v_2}{\sqrt{2}} Y_2^d \\ \Rightarrow Y_2^d &= \frac{\sqrt{2}}{v_2}\big(m_d - Pm_d\big), && (3.28) \\ (Y_3^d)_{33} P &= Y_3^d. && (3.29) \end{aligned}$$

Now that we have found the useful set of relations given in 3.29, we are ready to study the couplings of down-type quarks with neutral scalar h_2 and then change to the mass basis

to estimate the size of FCNCs in the down sector

$$\begin{aligned}\mathcal{L}_{\rm Y} &\supset \frac{1}{\sqrt{2}}\overline{d}_{La}d_{Rb}\Big[Y^d_{1ab}\frac{v_3}{v_{13}} - Y^d_{3ab}\frac{v_1}{v_{13}}\Big]h_2 + h.c.\\ &= \frac{1}{\sqrt{2}}\overline{d}_L\Big[Y^d_1\frac{v_3}{v_{13}} - Y^d_3\frac{v_1}{v_{13}}\Big]d_R h_2 + h.c.\\ &= \frac{1}{\sqrt{2}}\frac{h_2}{v_{13}}\overline{d}_L U^{d\dagger}_L U^d_L\Big[\frac{v_3}{\sqrt{2}}Y^d_1 - \frac{v_1}{\sqrt{2}}Y^d_3\Big]U^{d\dagger}_R U^d_R d_R + h.c.\\ &= \frac{h_2}{v}\overline{d'}_L\Big[\mathcal{N}^2_d\Big]d'_R + h.c.,\end{aligned} \tag{3.30}$$

where the primed physical states $d'_{L,R}$ and the FCNC matrix $\mathcal{N}^2_d$ are given by

$$d'_{L,R} = U^d_{L,R}d_{L,R}, \qquad \overline{d'}_{L,R} = \overline{d}_{L,R}U^{d\dagger}_{L,R}, \tag{3.31}$$

$$\mathcal{N}^2_d \equiv \frac{v}{v_{13}}U^d_L\Big[\frac{v_3}{\sqrt{2}}Y^d_1 - \frac{v_1}{\sqrt{2}}Y^d_3\Big]U^{d\dagger}_R, \tag{3.32}$$

where the matrix $\mathcal{N}^2_d$ is the FCNC strength matrix corresponding to the couplings to the neutral Higgs h_2. It is now possible to re-write $\mathcal{N}^2_d$ to see the dependence of the FCNC matrix on the Yukawa matrix elements and the physical masses in $m^d_{\rm diag}$. By performing the corresponding substitutions one gets

$$\begin{aligned}\mathcal{N}^2_d &= \frac{v}{v_{13}}U^d_L\Big[\frac{v_3}{\sqrt{2}}\Big(\frac{\sqrt{2}}{v_1}Pm_d - \frac{v_3}{v_1}Y^d_3\Big) - \frac{v_1}{\sqrt{2}}Y^d_3\Big]U^{d\dagger}_R\\ &= \frac{vv_3}{v_{13}v_1}U^d_L(Pm_d)U^{d\dagger}_R - \frac{1}{\sqrt{2}}\Big(\frac{v_3^2}{v_1}+v_1\Big)\frac{v}{v_{13}}(Y^d_3)_{33}U^d_L(P)U^{d\dagger}_R.\end{aligned} \tag{3.33}$$

Writing down each term in components and using the definition of the projector P e.g. $(P)_{ab} = \delta_{3a}\delta_{3b}$ we get for the first term in $\mathcal{N}^1_d$

$$\begin{aligned}U^d_L(Pm_d)U^{d\dagger}_R &= (U^d_L P U^{d\dagger}_L)(U^d_L m_d U^{d\dagger}_R)\\ &= (U^d_L)_{ab}\delta_{3a}\delta_{3d}(U^{d\dagger}_L)_{cd}(m^d_{\rm diag})_{ad}\\ &= (U^d_L)_{3b}(U^{d\dagger}_L)_{c3}(m^d_{\rm diag})_{ad}.\end{aligned}$$

Then, it is straightforward to see that

$$(\mathcal{N}^2_d)_{bc} = \frac{vv_3}{v_{13}v_1}(U^d_L)_{3b}(U^{d\dagger}_L)_{c3}(m^d_{\rm diag})_{ad} - \frac{1}{\sqrt{2}}\Big(\frac{v_3^2}{v_1}+v_1\Big)\frac{v}{v_{13}}(Y^d_3)_{33}(U^d_L)_{3b}(U^{d\dagger}_R)_{c3}. \tag{3.34}$$

Finally, recalling that elements $(U^d_L)_{3i}$ (with $i = 1,2,3$) are fixed by relations (3.24) one arrives at

$$(\mathcal{N}^2_d)_{ij} = \frac{vv_3}{v_{13}v_1}V^*_{ti}V_{tj}(m^d_{\rm diag})_{jj} - \frac{1}{\sqrt{2}}\Big(\frac{v_3^2}{v_1}+v_1\Big)\frac{v}{v_{13}}(Y^d_3)_{33}V_{ti}(U^{d\dagger}_R)_{j3}, \tag{3.35}$$

where V_{ti} are the elements of CKM involving top-quarks and the phase e^{ia} has canceled out, as expected. To get intuition about the size of $(U_R^{d\dagger})_{j3}$, let us notice that if Y_1^d had no off-diagonal entries, then $(U_R^{d\dagger})_{j3}$ could be assumed to be block-diagonal as well. This means that assuming small Y_1^d off-diagonal entries one obtains an accordingly small $\mathcal{N}_d^2$ matrix.

A similar analysis follows for h_3 couplings to estimate $\mathcal{N}_d^3$. Writing down directly the Yukawa couplings in terms of the physical down-quark states one gets

$$\mathcal{L}_{\rm Y} \supset \frac{h_3}{v}\overline{d'}_L\Big[\mathcal{N}_d^3\Big]d'_L + h.c., \tag{3.36}$$

where the primed states are given in (3.31) and $\mathcal{N}_d^3$ is defined as

$$\mathcal{N}_d^3 \equiv U_L^d\Big[\frac{v_2}{vv_{13}}\big(\frac{v_1}{\sqrt{2}}Y_1^d + \frac{v_3}{\sqrt{2}}Y_3^d\big) - \frac{v_{13}}{\sqrt{2}v}Y_2^d\Big]v_L^{d\dagger}. \tag{3.37}$$

Using the projector P definition (3.25) and the fixed elements of U_L^d, one arrives at the following expression for $\mathcal{N}_d^3$

$$\begin{aligned}
\mathcal{N}_d^3 &= U_L^d\Big[\frac{v_2}{vv_{13}}(Pm_d) - \frac{v_{13}}{vv_2}(m_d - Pm_d)\Big]U_L^{d\dagger} \\
&= U_L^d\Big[\Big(\frac{v_2}{vv_{13}} + \frac{v_3}{vv_2}\Big)Pm_d - \frac{v_{13}}{vv_2}m_d\Big]U_L^{d\dagger} \\
\Rightarrow (\mathcal{N}_d^3)_{ij} &= \Big(\frac{v_2}{vv_{13}} + \frac{v_{13}}{vv_2}\Big)V_{ti}^*V_{tj}(m_{\rm diag}^d)_{jj} - \frac{v_{13}}{vv_2}(m_{\rm diag}^d)_{jj}.
\end{aligned} \tag{3.38}$$

Let us notice that, for instance, the coupling of neutral h_3 with down-type quarks as given by (3.38) is controlled by the factor $|V_{td}V_{ts}^*| = |A^2\lambda^5(\rho - i\eta)| \approx 10^{-3}$ (for $i = 1, j = 2$) where λ, A are the Wolfenstein parameters in (2.4.1). This means that a suppression of 10^{-3} is, at least theoretically, provided by having imposed a family symmetry in the BGL style.

The flavour structure of the 3HDM model presented in this paper is characterized by the mass matrices m^d, m^u and the strength matrices of the tree-level FCNCs $\mathcal{N}_d^2, \mathcal{N}_d^3$. In particular, since the lightest SM-like Higgs is required to be in the alignment limit [31] it will not have contributions to tree-level FCNCs (see Appendix B for the general expressions of some interactions mediated by non-SM scalars). The alignment limit sets conditions on the scalar sector of our model enforcing that the lightest Higgs doublet H_1 acquires the SM VEV v, which results in a SM-like Higgs state in the particle spectra.

3.3 The scalar sector

In this section, we describe the general structure of the scalar potential under the $\mathrm{U}(1)\times\mathrm{Z}_2$ family symmetry and the consequences of imposing the alignment limit. Some of the known problems that 3HDM models encounter are the incomplete classification of symmetries that incorporate continuous symmetry groups, the different symmetry breaking patterns

and also, the many different vacuum alignments that could be realisable in a 3HDM. As mentioned before, in this thesis we impose a family $\mathrm{U}(1) \times \mathrm{Z}_2$ symmetry, which is one of the few known possible symmetries of 3HDMs [32].

The scalar potential of our 3HDM can be split in a part V_0 transforming under any phase rotation, a part transforming under the symmetry group G and soft breaking contribution. Typically, the scalar potential in 3HDMs is invariant under a symmetry G which is a subgroup of $G_0 = \mathrm{PSU}(3) \simeq \mathrm{SU}(3)/\mathrm{Z}_3$ [32],

$$V = V_0 + V_G + V_{\text{soft}}. \tag{3.39}$$

In our model, the symmetry G of the scalar potential is $\mathrm{U}(1) \times \mathrm{Z}_2$. The terms belonging to V_G which are allowed by the global $\mathrm{U}(1) \times \mathrm{Z}_2$ are

$$V_G = \lambda_{10}(H_1^\dagger H_3 H_1^\dagger H_3 + H_3^\dagger H_1 H_3^\dagger H_1). \tag{3.40}$$

Furthermore, the soft-breaking term contained in V_{soft} is defined in terms of the real soft-breaking mass m_{23}^2

$$V_{\text{soft}} = m_{23}^2(H_2^\dagger H_3 + H_3^\dagger H_2), \tag{3.41}$$

where the term in V_{soft} only breaks U(1) but not Z_2 preventing the appearance of a massless Goldstone boson. Since the potential needs to be Hermitian, the term $m_{23}^2 H_2^\dagger H_3$ alone cannot achieve hermiticity of the potential and one needs to add a second contribution to ensure this, namely $m_{23}^2(H_2^\dagger H_3 + H_3^\dagger H_2)$.

The terms belonging to the phase invariance part V_0 are

$$\begin{aligned} V_0 = {} & m_1^2 H_1^\dagger H_1 + m_2^2 H_2^\dagger H_2 + m_3^2 H_3^\dagger H_3 \\ & + \lambda_1 H_1^\dagger H_1 H_1^\dagger H_1 + \lambda_2 H_2^\dagger H_2 H_2^\dagger H_2 + \lambda_3 H_3^\dagger H_3 H_3^\dagger H_3 \\ & + \lambda_4 H_1^\dagger H_1 H_2^\dagger H_2 + \lambda_5 H_1^\dagger H_1 H_3^\dagger H_3 + \lambda_6 H_2^\dagger H_2 H_3^\dagger H_3 \\ & + \lambda_7 H_1^\dagger H_2 H_2^\dagger H_1 + \lambda_8 H_1^\dagger H_3 H_3^\dagger H_1 + \lambda_9 H_2^\dagger H_3 H_3^\dagger H_2, \end{aligned} \tag{3.42}$$

where λ_{1-10} are real numbers, otherwise explicit $\mathcal{CP}$-violation would be introduced. In order to stay within the perturbative regime, we have imposed the constraint $|\lambda_{1-10}| < 4\pi$ on the quartic terms, which is approximately the largest value that one can imagine for $|\lambda_{1-10}|$ without the theory becoming non-perturbative. For the scalar potential V to have a stable vacuum, as it is realized in nature, it needs to satisfy *boundness from below* conditions that will ensure that there is indeed an absolute minimum of energy. For 3HDMs, general expressions to ensure *boundness from below* are typically not easy to obtain. Therefore, as a first study of the model, we do not impose stability conditions, allowing for a wide range of quartic terms which will need to be constrained for future studies.

Given the potential V described in (3.42) critical points of the potential can be found. In practice, one requires the first derivatives of V to vanish in the vacuum,

$$\left(\frac{\partial V}{\partial H_i}\right)_{H_i = \langle H_i \rangle} = 0, \tag{3.43}$$

where we have assumed that the VEVs v_j are non-vanishing and that they are all different from each other[7]. The i-th Higgs doublet evaluated at vacuum is

$$\langle H_i \rangle = \begin{pmatrix} 0 \\ \frac{v_i}{\sqrt{2}} \end{pmatrix}, \tag{3.44}$$

where spontaneous $\mathcal{CP}$-violation is not introduced in this model since v_i are assumed to be real-valued quantities. Computing the first derivatives of the potential V with respect to the $\mathcal{CP}$-even fields results in the following expressions,

$$\frac{\partial V}{\partial \phi_1} = \frac{1}{2} v_1 \Big(\Big(2\lambda_{10} + \lambda_5 + \lambda_8 \Big) v_3^2 + 2 \Big(\lambda_1 v_1^2 + m_1^2 \Big) + \Big(\lambda_4 + \lambda_7 \Big) v_2^2 \Big), \tag{3.45}$$

$$\frac{\partial V}{\partial \phi_2} = \frac{1}{2} v_2 \Big(2 \Big(\lambda_2 v_2^2 + m_2^2 \Big) + \Big(\lambda_4 + \lambda_7 \Big) v_1^2 + \Big(\lambda_6 + \lambda_9 \Big) v_3^2 \Big) + m_{23}^2 v_3, \tag{3.46}$$

$$\frac{\partial V}{\partial \phi_3} = \frac{1}{2} \Big(\Big(2\lambda_{10} + \lambda_5 + \lambda_8 \Big) v_1^2 + 2 m_3^2 + \Big(\lambda_6 + \lambda_9 \Big) v_2^2 \Big) v_3 + \lambda_3 v_3^3 + m_{23}^2 v_2, \tag{3.47}$$

By requiring that the derivatives of the potential vanish for some value of the $\mathcal{CP}$-even fields ϕ_i, one arrives at the so-called *tadpole* equations of the model. The quadratic terms m_i^2 can be traded for the VEVs v_i after requiring that the potential has an absolute minimum. The scalar potential V is then parametrized by λ_{1-10}, m_{23}^2 and the VEVs.

Using the tadpole equations and expanding H_j around the vacuum

$$H_j = \begin{pmatrix} H_j^+ \\ \frac{1}{\sqrt{2}} (\phi_j + i\sigma_j + v_j) \end{pmatrix}, \quad H_j^\dagger = \begin{pmatrix} H_j^- & \frac{1}{\sqrt{2}} (\phi_j - i\sigma_j + v_j) \end{pmatrix}, \tag{3.48}$$

one arrives at the mass spectrum of the scalar, pseudo-scalar and charged scalar fields. The mass matrix of the neutral scalars in the gauge basis (ϕ_1, ϕ_2, ϕ_3) is parametrized by the quartic couplings λ_{1-10}, one soft-breaking term m_{23}^2 and three VEVs v_i. The explicit form of m_h^2 is the following

$$m_h^2 = \begin{pmatrix} m_{\phi_1\phi_1} & \Big(\lambda_4 + \lambda_7 \Big) v_1 v_2 & \Big(2\lambda_{10} + \lambda_5 + \lambda_8 \Big) v_1 v_3 \\ \Big(\lambda_4 + \lambda_7 \Big) v_1 v_2 & m_{\phi_2\phi_2} & \Big(\lambda_6 + \lambda_9 \Big) v_2 v_3 + m_{23}^2 \\ \Big(2\lambda_{10} + \lambda_5 + \lambda_8 \Big) v_1 v_3 & \Big(\lambda_6 + \lambda_9 \Big) v_2 v_3 + m_{23}^2 & m_{\phi_3\phi_3} \end{pmatrix}, \tag{3.49}$$

where the diagonal terms are given by

$$\begin{aligned} m_{\phi_1\phi_1} &= \frac{1}{2} \Big(\Big(2\lambda_{10} + \lambda_5 + \lambda_8 \Big) v_3^2 + 6\lambda_1 v_1^2 + \Big(\lambda_4 + \lambda_7 \Big) v_2^2 \Big) + m_1^2, \\ m_{\phi_2\phi_2} &= \frac{1}{2} \Big(6\lambda_2 v_2^2 + \Big(\lambda_4 + \lambda_7 \Big) v_1^2 + \Big(\lambda_6 + \lambda_9 \Big) v_3^2 \Big) + m_2^2, \\ m_{\phi_3\phi_3} &= \frac{1}{2} \Big(\Big(2\lambda_{10} + \lambda_5 + \lambda_8 \Big) v_1^2 + 6\lambda_3 v_3^2 + \Big(\lambda_6 + \lambda_9 \Big) v_2^2 \Big) + m_3^2. \end{aligned} \tag{3.50}$$

[7] A priori, this is not a necessary requirement.

The pseudo-scalar mass matrix has a somewhat simpler structure than m_h^2, see for example that $m_{A^0}^2$ in the gauge basis $(\sigma_1, \sigma_2, \sigma_3)$ takes the following form

$$m_{A^0}^2 = \begin{pmatrix} m_{\sigma_1\sigma_1} & 0 & 2\lambda_{10}v_1v_3 \\ 0 & m_{\sigma_2\sigma_2} & m_{23}^2 \\ 2\lambda_{10}v_1v_3 & m_{23}^2 & m_{\sigma_3\sigma_3} \end{pmatrix}, \tag{3.51}$$

where the diagonal elements are given also as functions of the scalar potential parameters, namely

$$\begin{aligned} m_{\sigma_1\sigma_1} &= \frac{1}{2}\Big(\Big(-2\lambda_{10}+\lambda_5+\lambda_8\Big)v_3^2 + 2\lambda_1 v_1^2 + \Big(\lambda_4+\lambda_7\Big)v_2^2\Big) + m_1^2, \\ m_{\sigma_2\sigma_2} &= \frac{1}{2}\Big(2\lambda_2 v_2^2 + \Big(\lambda_4+\lambda_7\Big)v_1^2 + \Big(\lambda_6+\lambda_9\Big)v_3^2\Big) + m_2^2, \\ m_{\sigma_3\sigma_3} &= \frac{1}{2}\Big(\Big(-2\lambda_{10}+\lambda_5+\lambda_8\Big)v_1^2 + 2\lambda_3 v_3^2 + \Big(\lambda_6+\lambda_9\Big)v_2^2\Big) + m_3^2. \end{aligned} \tag{3.52}$$

Finally, the last mass matrix of the scalar sector in the one corresponding to the charged scalar fields H_k^+. In the gauge basis we have

$$m_{H^-}^2 = \begin{pmatrix} m_{H_1^- H_1^+} & \frac{1}{2}\lambda_7 v_1 v_2 & \frac{1}{2}\Big(2\lambda_{10}+\lambda_8\Big)v_1v_3 \\ \frac{1}{2}\lambda_7 v_1 v_2 & m_{H_2^- H_2^+} & \frac{1}{2}\lambda_9 v_2 v_3 + m_{23}^2 \\ \frac{1}{2}\Big(2\lambda_{10}+\lambda_8\Big)v_1v_3 & \frac{1}{2}\lambda_9 v_2 v_3 + m_{23}^2 & m_{H_3^- H_3^+} \end{pmatrix}, \tag{3.53}$$

where the diagonal terms are

$$\begin{aligned} m_{H_1^- H_1^+} &= \frac{1}{2}\Big(2\lambda_1 v_1^2 + \lambda_4 v_2^2 + \lambda_5 v_3^2\Big) + m_1^2, \\ m_{H_2^- H_2^+} &= \frac{1}{2}\Big(2\lambda_2 v_2^2 + \lambda_4 v_1^2 + \lambda_6 v_3^2\Big) + m_2^2, \\ m_{H_3^- H_3^+} &= \frac{1}{2}\Big(2\lambda_3 v_3^2 + \lambda_5 v_1^2 + \lambda_6 v_2^2\Big) + m_3^2. \end{aligned} \tag{3.54}$$

The rotation matrices that will bring the scalar mass matrices $m_h^2, m_{A^0}^2, m_{H^-}^2$ into a diagonal form are Z^H, Z^A, Z^+, respectively, where the diagonalization is given by

$$\begin{aligned} Z^H m_h^2 (Z^H)^\dagger &= m_h^{2,diag}, \\ Z^A m_{A^0}^2 (Z^A)^\dagger &= m_{A^0}^{2,diag}, \\ Z^+ m_{H^-}^2 (Z^+)^\dagger &= m_{H^-}^{2,diag}. \end{aligned} \tag{3.55}$$

The scalar fields in the gauge basis are related to the mass-eigenstates by the rotation matrices Z^{H,A^0,H^-}, respectively

$$\phi_k = \sum_j Z_{jk}^H H_j, \quad \sigma_k = \sum_j Z_{jk}^A A_j^0, \quad H_k^+ = \sum_j Z_{jk}^+ H_j^{+\prime}. \tag{3.56}$$

Before imposing the alignment limit, we rotate our mass matrices from the gauge basis to the Higgs basis[8], making explicit the presence of three massless Goldstone bosons. The alignment limit forces the vacuum in the SM direction. As a result, the lightest scalar Higgs in our 3HDM is a linear combination of the unphysical $\mathcal{CP}$-even scalar fields ϕ_i weighted by the three VEVs in a very special way:

$$h_1 = \frac{1}{v}\big(v_1\phi_1 + v_2\phi_2 + v_3\phi_3\big). \tag{3.57}$$

In practice, this alignment is achieved by introducing the rotation matrix $\mathcal{O}_{\psi_1\psi_2}$ defined in (3.9). Transforming the squared mass matrices $m^2_{H^\pm}, m^2_{A^0}, m^2_h$ by rotating by $\mathcal{O}_{\psi_1\psi_2}$, the pseudo-scalar and the charged scalar Higgs mass matrices become block-diagonal

$$\begin{aligned} m'^2_{H^\pm} &= \mathcal{O}_{\psi_1\psi_2} m^2_{H^\pm} \mathcal{O}^T_{\psi_1\psi_2}, \\ m'^2_{A^0} &= \mathcal{O}_{\psi_1\psi_2} m^2_{A^0} \mathcal{O}^T_{\psi_1\psi_2}, \\ m'^2_{h} &= \mathcal{O}_{\psi_1\psi_2} m^2_{h} \mathcal{O}^T_{\psi_1\psi_2}. \end{aligned}$$

After the rotation, the $m'^2_{H^\pm}$ matrix has the following structure,

$$\begin{aligned} m'^2_{H^\pm}(1,1) &= 0, \quad m'^2_{H^\pm}(1,2) = 0, \quad m'^2_{H^\pm}(1,3) = 0\,, \\ m'^2_{H^\pm}(2,2) &= -\frac{1}{4}v^2\cos^2\psi_1(\lambda_7+\lambda_8+2\lambda_{10}+(-\lambda_7+\lambda_9+2\lambda_{10})\cos 2\psi_2) \\ &\quad -\frac{1}{2}\sin\psi_1\big(v^2(\lambda_8+2\lambda_{10})\cos^2\psi_2\sin\psi_1 + v^2\lambda_9\sin\psi_1\sin^2\psi_2 \\ &\quad -2m^2_{23}\tan\psi_1\tan\psi_2\big)\,, \\ m'^2_{H^\pm}(2,3) &= \frac{1}{2}\sin\psi_1\big(-2m^2_{23}\sec\psi_2 + v^2(-\lambda_7+\lambda_9)\cos\psi_1\sin\psi_2\big)\,, \\ m'^2_{H^\pm}(3,3) &= \frac{1}{4}\Big(v^2(\lambda_7-\lambda_9)\cos^2\psi_1 + 4m^2_{23}\cos\psi_1\csc\psi_2\sec\psi_2 \\ &\quad -v^2\big(\lambda_7+\lambda_9+(\lambda_7-\lambda_9)\sin^2\psi_1\big)\Big)\,. \end{aligned} \tag{3.58a}$$

Rotating the mass matrix of the pseudo-scalar Higgs field one gets

$$\begin{aligned} m'^2_{A^0}(1,1) &= 0, \quad m'^2_{A^0}(1,2) = 0, \quad m'^2_{A^0}(1,3) = 0\,, \\ m'^2_{A^0}(2,2) &= -2v^2\lambda_{10}\cos^4\psi_1\cos^2\psi_2 + \sin\psi_1\big(-v^2\lambda_{10}(3+\cos 2\psi_1)\cos^2\psi_2\sin\psi_1\,, \\ &\quad +m^2_{23}\tan\psi_1\tan\psi_2\big)\,, \\ m'^2_{A^0}(2,3) &= -m^2_{23}\sec\psi_2\sin\psi_1\,, \\ m'^2_{A^0}(3,3) &= 2m^2_{23}\cos\psi_1\csc 2\psi_2\,. \end{aligned} \tag{3.59a}$$

[8] An intermediate basis between the gauge and the physical basis.

Finally, rotating the mass matrix of the scalar Higgs field results in the only non-block-diagonal mass matrix. For brevity, only the first column of $m_h'^2$ is shown here,

$$\begin{aligned}
m_h'^2(1,1) &= 2v^2 \sin\psi_2 \Big(\lambda_3 \cos^4\psi_1 \cos^3\psi_2 \cot\psi_2 + \lambda_1 \cos^3\psi_2 \cot\psi_2 \sin^4\psi_1 \\
&\quad + (\lambda_4+\lambda_7)\cos^2\psi_2 \sin^2\psi_1 \sin\psi_2 + \lambda_2 \sin^3\psi_2 \\
&\quad + \cos^2\psi_1 \cos^2\psi_2 \big((\lambda_5+\lambda_8+2\lambda_{10}) \cos\psi_2 \cot\psi_2 \sin^2\psi_1 + (\lambda_6+\lambda_9)\sin\psi_2 \big) \Big), \\
m_h'^2(1,2) &= v^2 \cos\psi_1 \cos\psi_2 \sin\psi_1 \big((\lambda_1 - \lambda_3 + (\lambda_5+\lambda_8+2\lambda_{10}-\lambda_1-\lambda_3)\cos 2\psi_1)\cos^2\psi_2 \\
&\quad + (\lambda_4 - \lambda_6 + \lambda_7 - \lambda_9)\sin^2\psi_2 \big), \\
m_h'^2(1,3) &= v^2 \cos\psi_2 \sin\psi_2 \Big(\cos^2\psi_2 \big(-\cos^2\psi_1 (\lambda_6+\lambda_9-2\lambda_3\cos^2\psi_1) \\
&\quad - (\lambda_4+\lambda_7-\lambda_1-2(\lambda_5+\lambda_8+\lambda_{10})\cos^2\psi_1 + \lambda_1\cos 2\psi_1)\sin^2\psi_1 \big) - 2\lambda_2 \sin^2\psi_2 \\
&\quad + \big((\lambda_6+\lambda_9)\cos^2\psi_1 + (\lambda_4+\lambda_7)\sin^2\psi_1 \big)\sin^2\psi_2 \Big).
\end{aligned} \tag{3.60a}$$

The alignment limit can be imposed on $m_h'^2$ in the Higgs basis, enforcing that the lightest Higgs h_1 acquires the VEV v. This will result in a neutral scalar Higgs h_1 with couplings to bosons and fermions very close to the SM Higgs boson. Furthermore, a set of parameters can be chosen self-consistently such that the mass of h_1 is 125 GeV. In practice, imposing the alignment limit in the Higgs basis translates to requiring that the following relations hold simultaneously for a given point in the parameter space

$$m_h^{2\prime}(1,1) = m_{125}^2, \tag{3.61}$$
$$m_h^{2\prime}(2,1) = 0, \tag{3.62}$$
$$m_h^{2\prime}(3,1) = 0. \tag{3.63}$$

In this way, the scalar mass matrix $m_h^{2\prime}$ is block-diagonal and the mass of the SM-Higgs h_{125} becomes an input parameter of the model.

Lastly, we include three angles $\delta_0, \delta_1, \delta_2$ to parametrize the full diagonalization of the mass matrices $m_{h,A^0,H^\pm}'^2$. To illustrate this, let us rotate the pseudo-scalar mass matrix $m_{A^0}'^2$ to the mass basis,

$$\mathrm{diag}(0, \mathrm{m}_{\mathrm{A}_1^0}^2, \mathrm{m}_{\mathrm{A}_2^0}^2) = \mathcal{O}_{\delta_1} \begin{pmatrix} 0 & & \\ & m_{A^0}'^2(2,2) & m_{A^0}'^2(2,3) \\ & m_{A^0}'^2(2,3) & m_{A^0}'^2(3,3) \end{pmatrix} \mathcal{O}_{\delta_1}^{\mathrm{T}}, \tag{3.64}$$

where we have defined the rotation matrix $\mathcal{O}_{\delta_1}$ in terms of the angle δ_1

$$\mathcal{O}_{\delta_1} = \begin{pmatrix} 1 & & \\ & \cos\delta_1 & -\sin\delta_1 \\ & \sin\delta_1 & \cos\delta_1 \end{pmatrix}, \tag{3.65}$$

or expressed in a more convenient form for our purposes,

$$m'^2_{A^0} = \mathcal{O}^T_{\delta_1} \mathrm{diag}(0, \mathrm{m}^2_{\mathrm{A}^0_1}, \mathrm{m}^2_{\mathrm{A}^0_2}) \mathcal{O}_{\delta_1}. \tag{3.66}$$

Here, we have parametrized the pseudo-scalar mass matrix $m'^2_{A^0}$ to avoid the explicit calculations of eigenvalues. A similar procedure is done to parametrize the scalar and charged mass matrices m'^2_h and $m'^2_{H^\pm}$. As expected, not all the aforementioned parameters are independent since they are related by the conditions of alignment, namely relations (3.63). For illustration, one of the quartic couplings λ_4 of the potential V is shown here (for more details see Appendix A)

$$\begin{aligned} \lambda_4 \;=\; & \frac{1}{2v^2}\Big(2m^2_{h_1} - 2m^2_{H_3}\cos^2\delta_0 + 4m^2_{H^\pm_2}\cos^2\delta_2 - m^2_{H_2}(2\sin^2\delta_0 + \cot\psi_1 \csc\psi_2 \sin 2\delta_0) \\ & + 4m^2_{H^\pm_1}\sin^2\delta_2 + \cot\psi_1\csc\psi_2(m^2_{H_3}\sin 2\delta_0 + 2(m^2_{H^\pm_1} - m^2_{H^\pm_2})\sin 2\delta_2)\Big), \end{aligned} \tag{3.67a}$$

and the soft-breaking term m^2_{23},

$$m^2_{23} = m^2_{A^0_1}\left\{\frac{\cos\psi_2 \sec\psi_1 \sin\psi_2}{\tan\psi_1 \sin\psi_2 \cot\delta_1 - 1}\right\}. \tag{3.68}$$

Additionally, the angle δ_1 is not a free parameter because it is completely determined by the masses. The following equation is solved if a set of masses and angles is provided

$$\sin\psi_2 \tan\psi_1 = -\frac{(m^2_{A^0_1} - m^2_{A^0_2})\tan\delta_1}{m^2_{A^0_1} + m^2_{A^0_2}\tan^2\delta_1}, \tag{3.69}$$

which is a quadratic equation in the variable $\tan\delta_1$ which can be easily solved.

Let us summarize what has been presented in this section. Given a set of mass matrices $m'^2_{h,A^0,H^\pm}$ in our 3HDM, one can parametrize them by rotating to the Higgs basis where the pseudo-scalar and the charged mass matrices are block-diagonal, making explicit the presence of three massless Goldstone bosons. Then, the alignment limit is imposed to ensure that the lightest scalar boson h_1 acquires the VEV v resulting in a SM-like scalar. Lastly, three rotation matrices are implemented to fully diagonalize the mass forms, resulting in a system equations for the scalar sector parameters. In the scalar sector, there is a total of 14 degrees of freedom, namely 10 quartic couplings λ_{10}, one soft breaking term m^2_{23} and three VEVs v_{1-3}. In this section, we have illustrated how one can trade these 14 degrees of freedom for 7 scalar masses $m^2_{125}, m^2_{H_{2,3}}, m^2_{H^\pm_{1,2}}, m^2_{A^0_{1,2}}$, the SM VEV v, two VEV angles ψ_1, ψ_2, two diagonalization angles $\delta_{0,2}$ and two alignment limit conditions.

To finish this section, let us stress that the alignment limit condition can be relaxed for future studies. A possible scenario worth studying in the future is the case where the alignment is not exact but a deviation from it is considered. Nevertheless, such an alignment limit condition offers a simple way of identifying physical states in the scalar sector, where one of them is the SM-Higgs state.

3.4 Flavour physics

Flavour physics seeks to disentangle the hidden mechanism by which flavour symmetry breaks and has played, together with $\mathcal{CP}$-violation, a crucial role in the construction of the SM. More than 50 years ago, Gell-Mann first noticed that there was an underlying SU(3) *flavour* symmetry governing mesonic and baryonic processes which brought him to consider the existence of u-, d-, and s-quarks as their fundamental ingredients [33]. Then, in order to explain the surprisingly small value of the $\Gamma(K_L \to \mu\overline{\mu})$ the c-quark was postulated [34]. As flavour physics matured, it was understood that the third generation of quarks was needed to explain the amount of detected $\mathcal{CP}$-violation in K^0 mixing [35]. Later, the t-quark mass was estimated before its discovery from $\mathcal{CP}$-violation in $K^0 - \overline{K}^0$ and $B^0 - \overline{B}^0$ transitions [36]. The importance of flavour physics lies in the fact that most of the parameters of the SM are in the Yukawa sector, making flavour- and $\mathcal{CP}$-violating decays excellent playgrounds for NP.

The flavour structure of the SM becomes more interesting at higher orders of perturbation: FCNCs are predicted to be small in the SM since they appear only at loop-level. This suppression of FCNCs has been confirmed by a great amount of processes involving quark-flavour-violating observables such as the leptonic and semi-leptonic decays of the B, D, K mesons. Furthermore, the hierarchy in the CKM matrix has been intensively measured through different experiments involving tree-level and loop-level contributions as well as $\mathcal{CP}$-violating and $\mathcal{CP}$-conserving processes. The excellent agreement of a great amount of meson decays on the determination of the CKM matrix points towards an active flavour hierarchical mechanism that is always present in flavour transitions.

Thus, the flavour structure of the SM needs to be reproduced by any model with extended Higgs sectors. The introduction of new fields, and therefore new parameters, could result in FCNCs that are not within the experimentally allowed bounds and lead to phenomenological inconsistencies. Flavour physics data will set stringent constraints on our 3HDM, most likely excluding regions in the parameter space where unwanted contributions from non-standard scalars dominate.

3.5 Confronting flavour data

In the case of models like 3HDMs, where extra Feynman diagrams need to be considered in addition to the SM ones, flavour experimental data imposes stringent constraints on the parameter space of our model. One can organize different processes that will lead to NP at tree- and loop level in the following list [26]:

- Reactions with tree-level NP contributions mediated by charged scalars $H^{\pm}_{2,3}$ and SM tree-level contributions mediated by $W^{\pm}$. For example, leptonic and semi-leptonic decays such as $B \to \tau\nu$ and $B \to D\tau\nu$ or $\tau \to M\nu$.

- Reactions with tree-level NP contributions mediated by the neutral scalars $H_{2,3}$:

- Loop level SM contributions to the process $K_L \to \mu\overline{\mu}$, $B_s \to \mu\overline{\mu}$ and $B^0 - \overline{B^0}$ oscillations.
- Extremely suppressed[9] loop level SM contributions to the process $\tau \to \mu\mu\overline{\mu}$ or $\mu \to ee\overline{e}$.

- Reactions with loop-level NP contributions:
  - Loop level SM contributions to the process $\overline{B} \to X_s\gamma$.
  - Extremely suppressed loop-level SM contributions to the process $\tau \to \mu\gamma$ or $\mu \to e\gamma$.

In table 1 a summary of the potentially relevant reactions is given [26]. In this thesis, we test our 3HDM model by including some of the observables related to EW, Higgs and flavour physics. Therefore, the masses of non-SM scalars, as well as values for the VEVs, will be strongly constrained not only by the provided flavour observables but also by Higgs and EW precision tests data.

	3HDM				SM	
	Charged $H^{\pm}_{1,2}$		Neutral $H_{2,3}$		Tree	Loop
	Tree	Loop	Tree	Loop		
$M \to \ell\overline{\nu}, M'\ell\overline{\nu}$	✓	✓		✓	✓	✓
$M^0 \to \ell_1\overline{\ell}_2$		✓	✓	✓		✓
$M^0 - \overline{M}^0$ oscillation		✓	✓	✓		✓
$\overline{B} \to X_s\gamma$		✓		✓		✓
EW precision		✓		✓		✓

Table 1: Types of relevant observables of our 3HDM [26]. Leading contributions are shown in red colored ticks, while subleading (negligible) ones in black ticks. Since lepton-flavour violation is not included in our implementation due to diagonal Y_1^e, one has that $\ell_1 = \ell_2 = \ell$.

3.5.1 Tree-level processes mediated by charged $H^{\pm}_{1,2}$

Since the inclusion of extra Higgs doublets results in new interactions mediated by exotic scalars, transitions that involve the charged $W^{\pm}$ boson will now receive contributions coming from charged $H^{\pm}_{1,2}$. Such transitions are [26]: leptonic decays of mesons $M \to \ell\nu$ and semi-leptonic decays of mesons $M \to M'\ell\nu$. Let us briefly illustrate the NP contributions present in these processes.

Semileptonic decays get tree-level contributions coming from virtual $H^{\pm}_{1,2}$. The effective

[9] Due to almost vanishing ν masses.

Process	Value	Unit	Accuracy
Branching ratios			
$\mathcal{BR}(B \to X_s\gamma)$	2.36 ± 0.23	10^{-4}	(6.8%)
$\mathcal{BR}(B^0 \to \mu\overline{\mu})$	$3.9\pm^{1.6}_{1.4}$	10^{-10}	(41%)
$\mathcal{BR}(B_s \to \mu\overline{\mu})$	$2.9\pm^{0.7}_{0.6}$	10^{-9}	(24%)
ΔM_{B_d}	0.506 ± 0.0019	ps^{-1}	(0.37%)
ΔM_{B_s}	17.757 ± 0.021	ps^{-1}	(0.11%)
$\mathcal{BR}(B \to X_s\ell\overline{\ell})$	5.84 ± 0.69	10^{-6}	(12%)
$\mathcal{BR}(K^+ \to \pi^+\nu\overline{\nu})$	1.7 ± 1.1	10^{-10}	(65%)

Table 2: Some relevant flavour violating observables given with their experimental uncertainty and their relative accuracy [9].

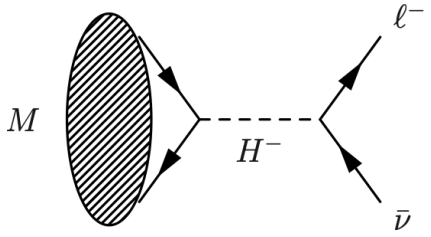

(a) Leptonic decay of a meson mediated by a charged Higgs.

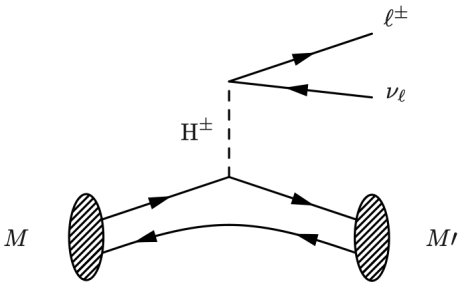

(b) Semi-leptonic decay of a meson mediated by a charged Higgs.

Lagrangian for semileptonic decays is given by

$$\mathcal{L}_{eff} = -\frac{4G_F}{\sqrt{2}} \sum_{u_i=u,c,t} \sum_{d_j=d,s,b} \sum_{\ell_a=e,\mu,\tau} \sum_{\nu_b=\nu_1,\nu_2,\nu_3} V_{u_i d_j} U_{\ell_a \nu_b}$$
$$\left\{ [\overline{u}_i \gamma^\mu \gamma_L d_j][\overline{\ell}_a \gamma_\mu \gamma_L \nu_b] + \left[\overline{u}_i \left(g_L^{u_i d_j \nu_b \ell_a} \gamma_L + g_R^{u_i d_j \nu_b \ell_a} \gamma_R \right) d_j \right] [\overline{\ell}_a \gamma_L \nu_b] \right\} + h.c., \quad (3.70)$$

where the quantities $g_L^{u_i d_j \nu_b \ell_a}$ and $g_R^{u_i d_j \nu_b \ell_a}$ are defined in terms of the Wilson coefficients $C^{u_i d_j}$, $C^{\nu_b \ell_a}$ and $C^{\ell_a \nu_b}$, namely

$$g_L^{u_i d_j \nu_b \ell_a} = \frac{m_{u_i} m_{\ell_a}}{m^2_{H^\pm_{1,2}}} C^{u_i d_j} C^{\nu_b \ell_a}, \quad g_R^{u_i d_j \nu_b \ell_a} = -\frac{m_{d_j} m_{\ell_a}}{m^2_{H^\pm_{1,2}}} C^{u_i d_j} C^{\ell_a \nu_b}. \quad (3.71)$$

The decay width of a leptonic decay $M \to \ell\overline{\nu}$ of a pseudo-scalar meson M with quarks $\overline{u}_i, d_j$ can be extracted from the effective Lagrangian above and is given by

$$\Gamma_0(M \to \ell\overline{\nu}) = G_F^2 m_\ell^2 f_M^2 |V_{u_i d_j}|^2 \frac{m_M}{8\pi} \left(1 - \frac{m_\ell^2}{m_M^2}\right)^2 \sum_{n=1,2,3} |U_{\ell\nu_n}|^2 |1 - \Delta^{\nu_n \ell}_{u_i d_j}|^2, \quad (3.72)$$

where, according to [37], for the B_d system one has $f_{B_d} = 190$ MeV and for the B_s system $f_{B_s} = 228$ MeV. Also, $\Delta_{u_i d_j}^{\nu_n \ell}$ is the new contribution coming from the new scalars $H_{1,2}^{\pm}$ and it is given by

$$\Delta_{u_i d_j}^{\nu_n \ell_a} = \frac{m_{u_i} m_{\ell_a}}{m_{H_{1,2}^{\pm}}^2} C^{u_i d_j} C^{\nu_n \ell_a}. \tag{3.73}$$

Since the process $M \to \ell\nu$ is helicity-suppressed in the SM and its decay rate is proportional to the mass of the fermions $m_{u_i} m_{\ell_a}$, interesting NP contributions will involve heavy mesons and the τ lepton e.g. $B \to \tau\nu, D_s \to \tau\nu$ [26].

3.5.2 Tree-level processes mediated by neutral $H_{2,3}$

While the NP processes mediated by $H_{1,2}^{\pm}$ from last section compete with tree-level SM amplitudes, neutral $H_{2,3}$ mediate tree-level processes which compete with loop-level SM contributions [26]. The types of processes are the following:

- $M^0 - \overline{M^0}$ oscillations, where M^0 could be the down-type mesons K^0, B_d^0, B_s^0 or the up-type meson D^0 (see figure 5).
- Rare decays $M^0 \to \ell_1 \ell_2$ (see figure 6).
- Lepton flavour violating (LFV) decays $\ell_1 \to \ell_2 \bar{\ell}_3 \ell_4$ which are not included in our implementation.

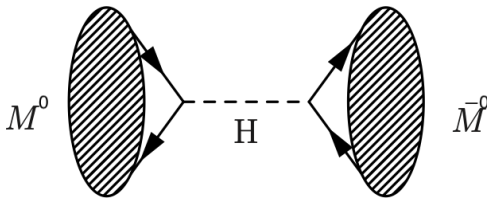

Figure 5: $M^0 - \overline{M^0}$ meson oscillation mediated by a neutral scalar Higgs.

$M^0 - \overline{M^0}$ oscillations The NP short-distance tree-level contribution to the amplitude of the transition of M^0 to $\overline{M^0}$ is given by [26]

$$\begin{aligned} M_{M,12}^{NP} = & \sum_{H_S = H_2, H_3} \frac{f_M^2 m_M}{96 v^2 M_{H_S}^2} \left(1 + \left(\frac{m_M}{m_{q_1} + m_{q_2}}\right)^2\right) C_1(H_S) \\ & - \sum_{H_P = A_1^0, A_2^0} \frac{f_M^2 m_M}{96 v^2 M_{H_P}^2} \left(1 + 11\left(\frac{m_M}{m_{q_1} + m_{q_2}}\right)^2\right) C_2(H_P), \end{aligned} \tag{3.74}$$

where m_M is the mass of a particular meson and $M_{H_{S,P}}$ are the masses of a neutral scalar and pseudo-scalar, respectively. The factors $C_{1,2}(H_{S,P})$ are the Wilson coefficients of the

corresponding interaction between non-SM Higgs states and the valence quarks $q_{1,2}$ of the meson M. Furthermore, here $C_1(H_S)$ and $C_2(H_P)$ correspond to the $\mathcal{CP}$-even and $\mathcal{CP}$-odd contributions to $M^{NP}_{M,12}$, respectively. The coefficients f_M depend on the type of meson e.g. for the K meson we have $f_K = 155.5$ MeV for a mass of $m_K = 497.614$ MeV [37]. For $B^0_d - \overline{B^0_d}$ and $B^0_s - \overline{B^0_s}$ systems, the differences in mass ΔM_{B_d} and ΔM_{B_s} are, to good approximation[10], given by

$$\Delta M_{B_d} = 2|M_{B_d,12}|, \quad \Delta M_{B_s} = 2|M_{B_d,12}|. \tag{3.75}$$

In the $K^0 - \overline{K^0}$ system, both quantities $M_{K,12}$ and $\Gamma_{K,12}$ play an important role in the determination of ΔM_K, therefore, NP contributions to $M_{K,12}$ must be such that the experimental value of the mass difference is not exceeded. Also, the $\mathcal{CP}$-violating observable ϵ_K [9]

$$|\epsilon_K| = \frac{\mathrm{Im(M_{K,12})}}{\sqrt{2}\Delta M_K}, \tag{3.76}$$

which, including higher order perturbative corrections and lattice QCD calculations [38], is estimated to be $|\epsilon_K|_{\mathrm{SM}} = (1.9 \pm 0.26) \times 10^{-3}$. This means that contributions coming from NP should not exceed 10% of its experimental value. In the case of the Kaon mass splitting, the experimental value is [9]

$$\Delta M_K = M_{K_L} - M_{K_S} = (3.484 \pm 0.006) \times 10^{-12}\ \mathrm{MeV}, \tag{3.77}$$

which corresponds to an experimental accuracy of approximately 0.17%.

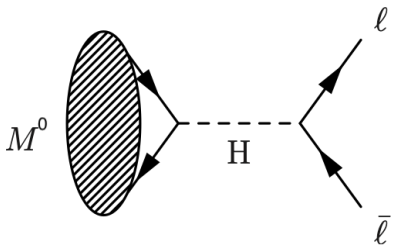

Figure 6: M^0 meson decay to a pair of charged leptons $\ell\bar{\ell}$ mediated by a neutral Higgs.

3.5.3 Loop level process $B \to X_s\gamma$

So far, only processes that have NP contributions at tree-level have been mentioned. Let us now briefly describe the loop-level decay $B \to X_s\gamma$, where the process at quark level is $b \to s\gamma$. The transition $b \to s\gamma$ is described by the following effective Hamiltonian computed at the energy scale $\mu_b = \mathcal{O}(m_b)$

$$\mathcal{H}_{eff}(b \to s\gamma) = -\frac{4G_F}{\sqrt{2}} V_{tb}V^*_{ts}\Big[C_7(\mu_b)Q_7 + C'_7(\mu_b)Q'_7 + C_8(\mu_b)Q_8 + C'_8(\mu_b)Q'_8\Big], \tag{3.78}$$

[10] valid for $M_{B_q,12} \gg \Gamma_{B_q,12}$ where $\Gamma_{B_q,12}$ is the absorptive transition amplitude.

where the primed operators $\mathcal{O}'_{7,8}$ are the new effective operators that are not present in the SM besides terms $\mathcal{O}(m_s/m_b)$. The factors $C_{7,8}(\mu_b)$ and $C'_{7,8}(\mu_b)$ are the Wilson coefficients of the dipole operators as discussed previously in section 2.5.2 and presented in equations (2.36) therein.

In our 3HDM, there will be NP contributions arising from processes mediated by charged $H^{\pm}_{2,3}$ and neutral $H_{2,3}$ Higgs fields (see figure 7). Although reactions mediated by neutral scalars can be naively expected to be small, because there is an enhancement due to the top quark mass (e.g. proportional to $m_t^2/m^2_{H^{\pm}_{2,3}}$ versus $m_b^2/m^2_{H_{2,3}}$) Feynman diagrams with FCNCs should not be neglected[11].

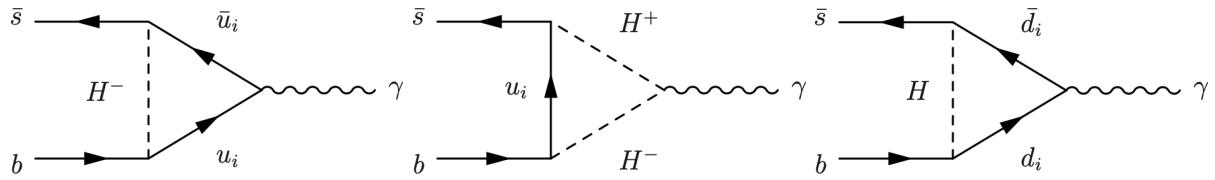

Figure 7: NP contribution to the transition $b \to s\gamma$ mediated by charged and neutral Higgs at loop-level.

3.6 Higgs physics

We briefly present the constraints imposed on the model coming from Higgs physics. The scans implement a stage of point selection according to the packages `HiggsBounds` (HB) and `HiggsSignals` (HS) [39][40], which where used after the numerical computations with `SPheno`[41][42].

One of the main ingredients in confronting Higgs data is `HiggsBounds`, which is a package that tests the theoretical predictions of our 3HDM against the exclusion bounds that have been set from Higgs searches at the LHC, LEP and the Tevatron. Some of the information regarding the experiment includes exclusion bounds at 95% C.L. on topological cross sections. After having specified the characteristics of our 3HDM, the implementation of `HiggsBounds` allows us to identify the most sensitive channel and verifies whether a given parameter point of the model is excluded at the 95% C.L.

A sister computer code of `HiggsBounds` is `HiggsSignals`, which can be easily implemented in the exclusion of parameter points. The computer code `HiggsSignals` is, therefore, a natural extension of `HiggsBounds` since both take as input the number of neutral Higgs bosons, scalar masses, cross sections, branching ratios, among other physical quantities. The basic experimental value that `HiggsSignals` uses is the *signal strength modifier* μ_{xx}, which parametrizes the signal rate of a particular final state xx, normalized to the SM expectation. Finally, `HiggsSignals` implements the peak-centered χ^2 method

[11] There could be a compensation coming from the values of the VEVs.

to determine quantitatively to what degree the data and the predicted theory of the model are compatible. The combined implementation of `HiggsBounds`/`HiggsSignals` looks at the properties of the discovered Higgs and searches for additional Higgs states, which are then either excluded or allowed in the particle spectra of our model. In our implementation of the 3HDM, we have found that all the points that pass `HiggsBounds` are extremely likely to pass `HiggsSignals` as well due to the alignment limit imposition.

3.7 Electroweak precision observables

In section 3.5 we have illustrated different flavour interactions at low energy that are capable of constraining the parameter space of our model e.g. certain values for the masses will be excluded due to large unwanted NP contributions, which can be clearly identified in the effective Hamiltonians of various QFV interactions. In addition to QFV data imposing constraints on new models, in section 3.6 we have also discussed how to study properties of new Higgs states and how to further constrain the parameter space based on Higgs searches physics. In addition to these constraints, EW precision observables should also be carefully studied and will play an important role in the exclusion of points in parameter space.

The oblique parameters S, T, U, which were first introduced by Peskin and T. Takeuchi [43], parametrize the effect of NP to EW radiative corrections. One can express the deviations of the observables with respect to the SM by defining $\Delta\mathcal{O}_i \equiv \mathcal{O}_i - \mathcal{O}_i^{SM} \rightarrow (\Delta S, \Delta T, \Delta U)$. Then, the requirement that contributions coming from new physics respect the EW precision tests within a 95% C.L. ellipsoid (see figure 8) can be imposed in the following way [44]

$$\Delta\chi^2 \equiv \sum_{ij} \left(\Delta\mathcal{O}_i - \Delta\mathcal{O}_i^{(0)}\right) \left[(\sigma^2)^{-1}\right]_{ij} \left(\Delta\mathcal{O}_j - \Delta\mathcal{O}_j^{(0)}\right) < 7.815, \tag{3.79}$$

where the covariance matrix is expressed in terms of the correlation matrix ρ_{ij} and the standard deviation σ_i of each parameter e.g. $\left[\sigma^2\right]_{ij} \equiv \sigma_i \rho_{ij} \sigma_j$. In order to test the oblique parameters, we implement results for the SM fit from the Gfitter collaboration [45]. The reference values $\Delta\mathcal{O}_i^{(0)}$ are computed by taking the mass of the SM Higgs scalar $m_{125} \approx 125$ GeV and the SM values for the oblique parameters $S_{\rm SM} = 0.05$, $T_{\rm SM} = 0.02$ and $U_{\rm SM} = 0.01$, as done by the authors in [45][44]. This leads to the following reference values for the S, T, U parameters

$$\Delta S^{(0)} = 0.08, \quad \Delta T^{(0)} = 0.05, \quad \Delta U^{(0)} = 0.02, \tag{3.80}$$

and the $(\sigma^2)^{-1}$ matrix

$$(\sigma^2)^{-1} = \begin{pmatrix} 867.49 & -904.30, & -360.66 \\ -904.30 & 1154.65 & 584.55 \\ -360.66 & 584.55 & 455.19 \end{pmatrix},$$

which are input in our χ^2 analysis in 3.79. The S, T, U ellipsoid condition in (3.79) was implemented as part of the scans. The package `SPheno` computes the deviations from

the SM prediction for the S, T, U oblique parameters. In the section 4.2, we show the points that passed not only the Higgs data constraints imposed by `HiggsBounds` and `HiggsSignals` but also EW precision tests, as described in this section.

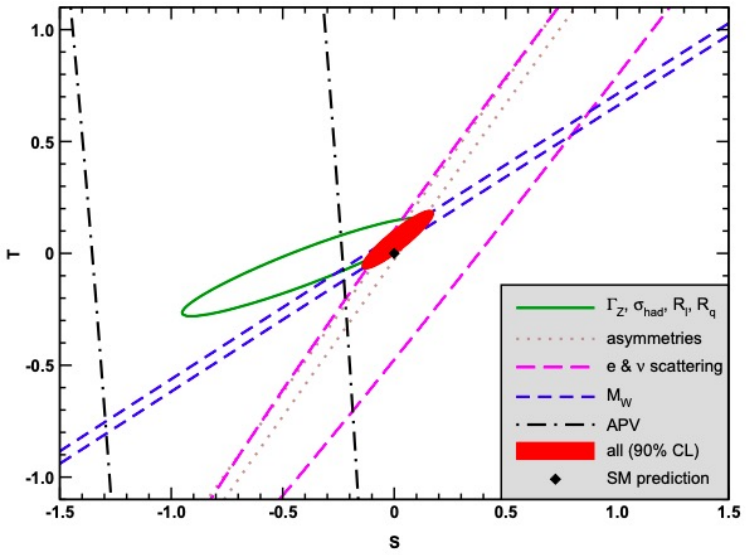

Figure 8: Figure from [9]: S and T offer a parametrization of the NP contributions in models with extended Higgs sectors.

4 Numerical analysis

The numerical calculations of the most important physical observables such as masses and decay rates of the new scalars, S, T, U oblique parameters, and QFV observables, were computed at different stages. An overview of this procedure is given here.

4.1 Methodology

The numerical analysis can be divided in the following stages:

1. Model building with `SARAH` [30].
2. Parametrization and pre-selection of suitable parameter-space points.
3. Implementation of `SPheno` [41][42].
4. Implementation `HiggsBounds` [39].
5. Implementation `HiggsSignals` [40].
6. Imposition of constraints coming from EW precision observables [44].

7. Implementation of `flavio` [46] to compute QFV observables.

In the following section we present the main results of this thesis where we have scanned over the free parameters of the model. Let us recall, in the scalar sector, there is a total of 14 degrees of freedom, according to section 3.3: 7 scalar masses $m^2_{125}, m^2_{H_{2,3}}, m^2_{H^{\pm}_{1,2}}, m^2_{A^0_{1,2}}$, the SM VEV v, two VEV angles ψ_1, ψ_2, two diagonalization angles $\delta_{0,2}$ and two alignment limit conditions.

For the masses we have scanned from 200 GeV to 5 TeV to, firstly, ensure that non-SM scalars are not extremely heavy and thus no renormalization group evolution is required and, secondly, to allow for relative light scalars that could be potentially discovered at current collider experiments. We have used $v = 246$ GeV, $\psi_{1,2}$ range from 0 to $\pi/2$ and the angles $\delta_{0,2}$ are defined from 0 to 2π.

Furthermore, we have presented the parametrization of the Yukawa sector, where there are 16 free parameters according to section 3.1: 9 fermion masses (at the top scale [47]) given in units of [GeV], namely $m_u = 0.00122$, $m_c = 0.590$, $m_t = 162.9$, $m_d = 0.0027$, $m_s = 0.052$, $m_b = 2.75$, $m_e = 0.00048$, $m_\mu = 0.1024$ and $m_\tau = 1.7421$; 4 Wolfenstein parameters in the CKM matrix, namely $A = 0.8080$, $\lambda = 0.22253$, $\overline{\rho} = 0.132$ and $\overline{\eta} = 0.341$ [9] and three angles $\chi_{1,2,3}$ which are allowed to range from 0 to 2π.

4.2 Results

In the previous subsections, we have shown a set of important physical observables that will constrain our 3HDM model by excluding parameter space points according to our implementation described in section 4.1. Such allowed regions in our 3HDM parameter space lead to NP contributions that respect the available experimental constraints. To verify the phenomenological consistency of our model, we need to identify further regions in the parameter space to be excluded by flavour physics data presented in section 3.5. Current experimental flavour data is presented in table 2 for some of the most relevant interactions, which will help to evaluate qualitatively whether our model respects experimental data and to what extent we are able to identify particularly interesting regions where all constraints are fulfilled. The results shown in this section, have passed all the aforementioned exclusion tests and reproduce a SM-like scalar Higgs boson with a mass of 125 GeV due to the alignment conditions. A detailed discussion about the QFV observables extracted from the `flavio` [46] python package takes place in what follows.

However, before discussing the main results of the phenomenological analysis of our model, a few words about the computation of flavour observables are needed. We have identified that `FlavorKit` [48] encounters issues in the estimation of some QFV observables, this is most likely due to a bug that needs attention for further computations. Nevertheless, we have identified that `SPheno` in conjunction with `FlavorKit` does compute correct Wilson coefficients that can be used to estimate QFV observables using an external computer code. We have chosen to use `flavio` to read the Wilson coefficients of our model to estimate a large number of flavour observables.

From our scans we have learned that our model respects all the flavour observables included in this thesis, which according to section 3.5, are the most relevant ones for models with extended Higgs sectors. We have computed the following set of QFV observables to identify regions capable of constraining our model: In the B meson system we have computed $\mathcal{BR}(B \to X_s\gamma)$, $\mathcal{BR}(B_0 \to \ell\overline{\ell})$, $\mathcal{BR}(B_s \to \ell\overline{\ell})$, ΔM_{B_s}, ΔM_{B_d}, $\mathcal{BR}(B^+ \to K^+\nu\overline{\nu})$, $\mathcal{BR}(B^+ \to \pi^+\nu\overline{\nu})$, $\mathcal{BR}(B^0 \to \pi^0\nu\overline{\nu})$, $\mathcal{BR}(B^0 \to K^0\nu\overline{\nu})$, $\mathcal{BR}(B^+ \to \overline{\ell}\nu)$, $\mathcal{BR}(B^+ \to D^0\overline{\ell}\overline{\nu})$, in the D meson system we have the leptonic decay $\mathcal{BR}(D^+ \to \overline{\ell}\nu)$ and finally, in the K meson system we have $\mathcal{BR}(K_L \to \overline{\mu}\mu)$, $\mathcal{BR}(K_L \to \overline{e}e)$, $\mathcal{BR}(K^+ \to \pi^+\overline{\nu}\nu)$, $\mathcal{BR}(K_L \to \pi^0\overline{\nu}\nu)$, ϵ_K and ϵ'/ϵ. From this set of QFV observables we present only the ones that show interesting correlations with the parameters of our model.

Let us describe regions for masses and VEVs that are allowed by Higgs data constraints and EW precision tests. In figures 9, 10, 11 and 12 we present the scalar masses that have passed the numerical scans. In figure 9, we show the masses of the different scalars mapped onto the space spanned by the two angles ψ_1 and ψ_2. We have found that allowed values for $\sin\psi_1$ are spread between 0.7 and 1, suggesting that there is a statistical hierarchy between the VEVs, typically we have that $v_1 > v_3$. On the other hand, small values of ψ_2 were preferred, pointing towards a general suppression $v_2 < v_1, v_3$.

Let us discuss the masses of non-SM scalars predicted by our model. First, it is important to mention that the labeling of the scalars is arbitrary e.g. simply by convention we have that $m_{H_2^\pm} \geq m_{H_1^\pm}$ and it would not change any physics if instead $m_{H_1^\pm}$ was heavier than $m_{H_2^\pm}$. Therefore, the points in figures 10, 11, 12 follow the $m_{H_3} \geq m_{H_2}$, $m_{A_2^0} \geq m_{A_1^0}$ and $m_{H_2^\pm} \geq m_{H_1^\pm}$ conventions, respectively.

One important characteristic of our results worth discussing is the presence of relatively light scalars. Our model predicts the presence of scalar masses around 300 GeV (see figures 10,11,12) which do not generate tensions with the SM predictions at first glance. Nevertheless, as we have learned in section 3.5, the couplings of non-SM scalars with the valence quarks of mesons are inversely proportional to the squared mass $m^2_{H_j}$ and it is expected that heavier scalars would lead to a phenomenologically safer scenario. However, as we will discuss in the next paragraphs, the model indeed allows for light non-SM scalars, whose corresponding QFV observables are in good agreement with the SM predictions.

Let us now look at allowed ST region as a result of the ellipsoid constraint in (3.79) that we discussed in section 3.7. Figures 13 and 14 show the S, T parameter points that have passes the HS/HB/EW-precision tests as functions of $\sin\psi_1$ and the lightest charged scalar mass $m_{H_1^\pm}$. Parameter points in 13 are centered around the value $S = -0.01$ and increasing values of $\sin\psi_1$ tend to be more spread out. Furthermore, parameter points with $\sin\psi_1$ close to unity correspond to light scalars shown in figure 14. Similarly, parameter points with a modest value of $\sin\psi_1$ result in heavier scalars of masses around 3000 GeV.

We now focus our attention to the QFV observables obtained from our scans, which are the main results of the work presented in this thesis: QFV observables validate the model suggesting that our 3HDM is phenomenological consistent. We show various branching ratios as functions of the VEV angle ψ_1 in the left panels of figures (15)-(21). In addition, we show in the right panels of figures (15)-(21), the dependence of QFV observables on the masses of $m_{H_1^\pm}$. For brevity, we do not show the equivalent figures for the other non-SM

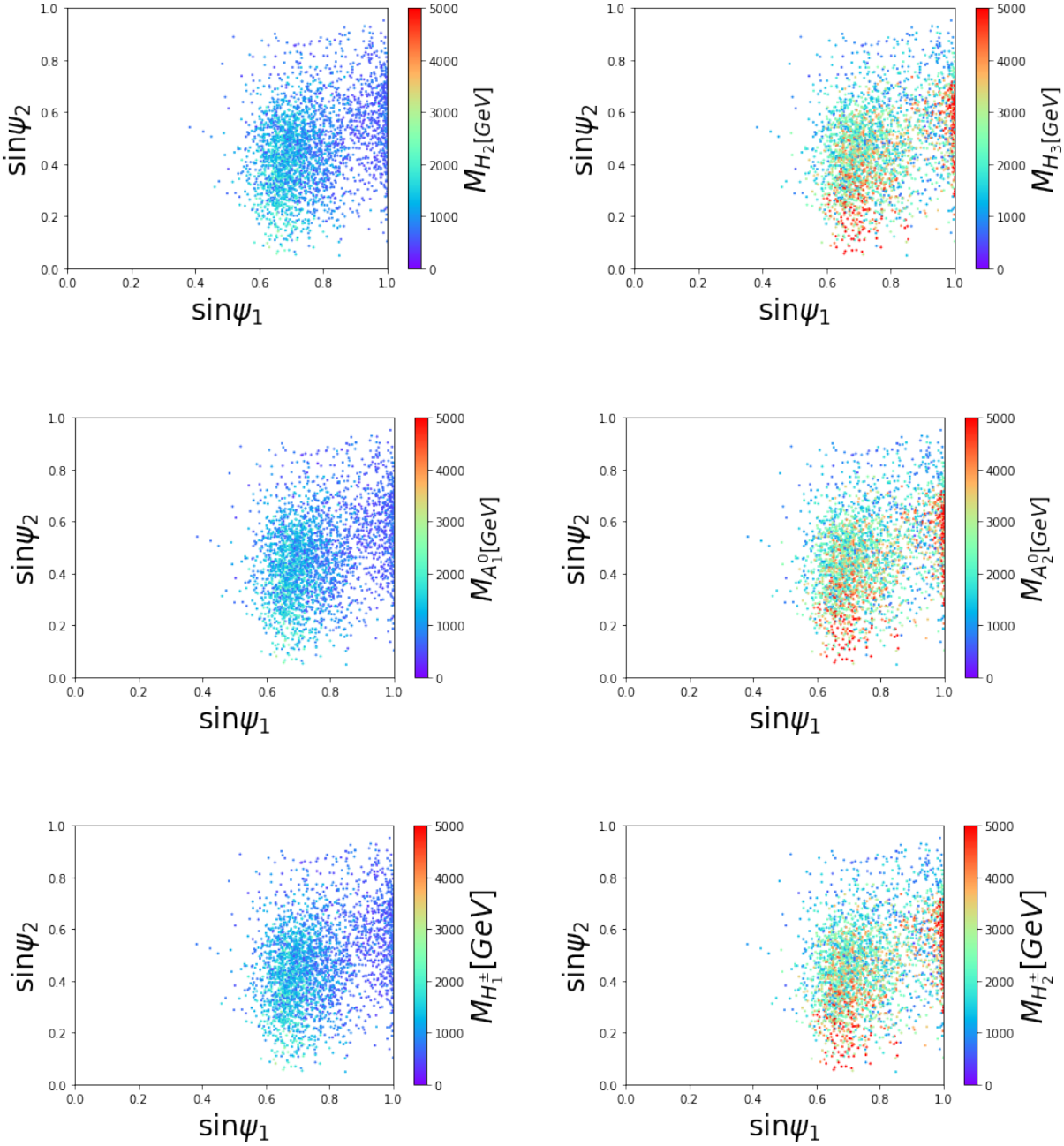

Figure 9: Masses of the neutral scalars $H_{2,3}$, pseudo-scalars $A^0_{1,2}$, and charged scalars $H^\pm_{1,2}$ in the space spanned by the VEV-angles ψ_1 and ψ_2.

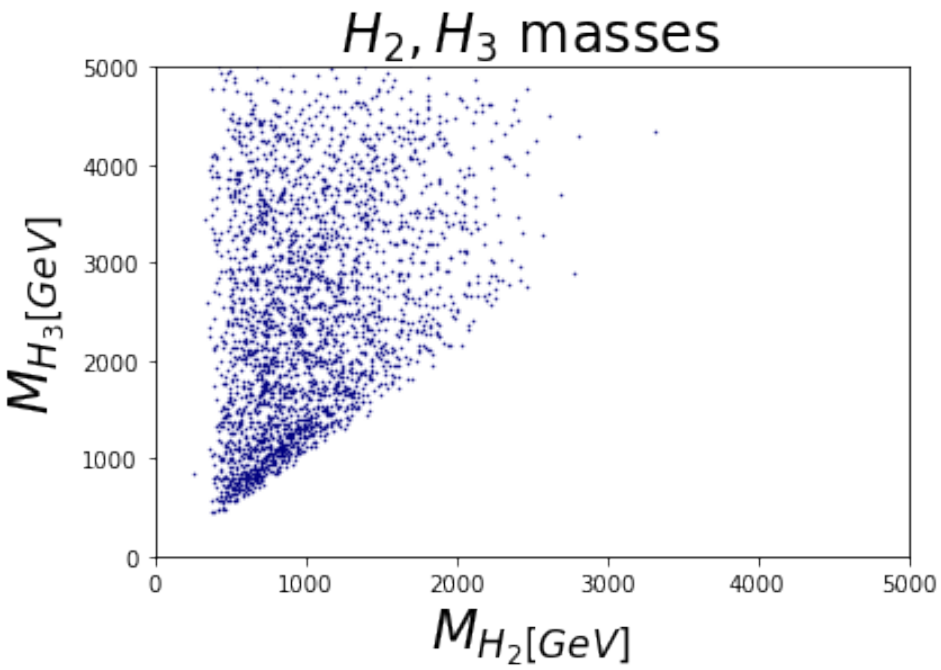

Figure 10: Distribution of non-SM neutral scalars $H_{2,3}$.

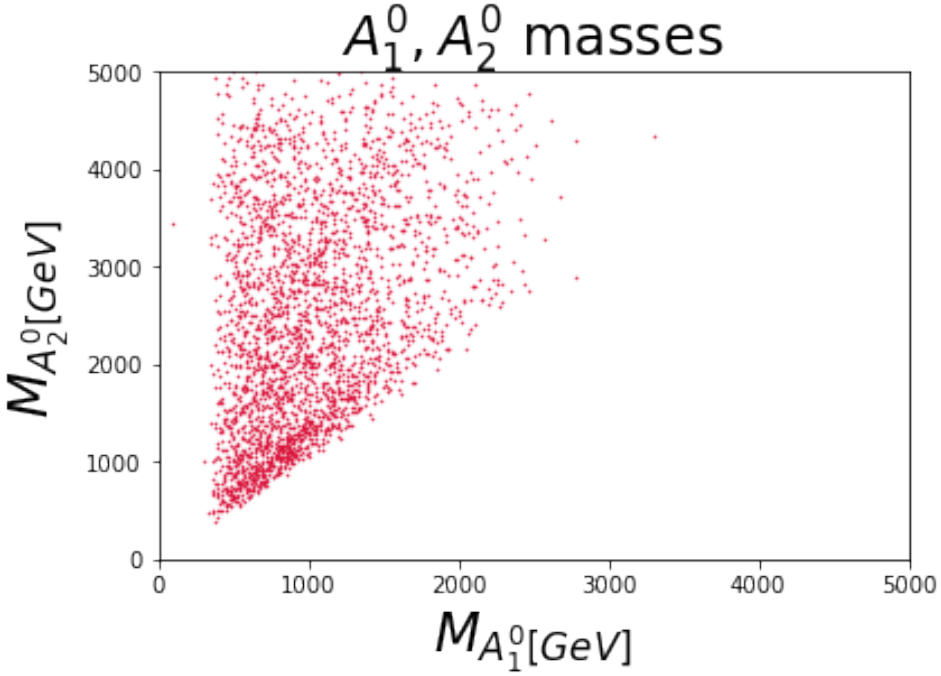

Figure 11: Distribution of non-SM neutral pseudo-scalars $A^0_{1,2}$.

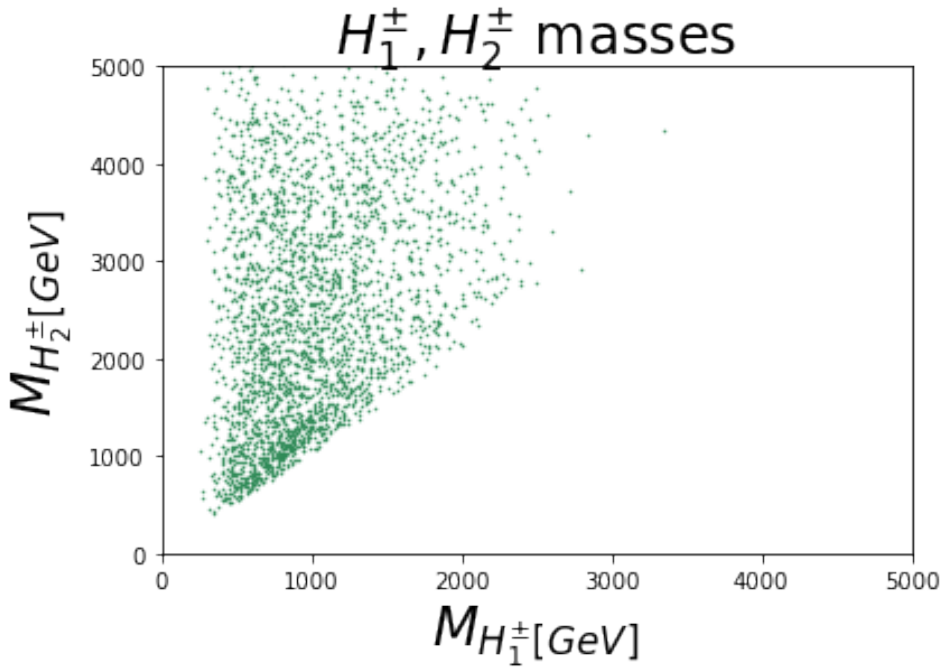

Figure 12: Distribution of non-SM charged scalars $H^{\pm}_{1,2}$.

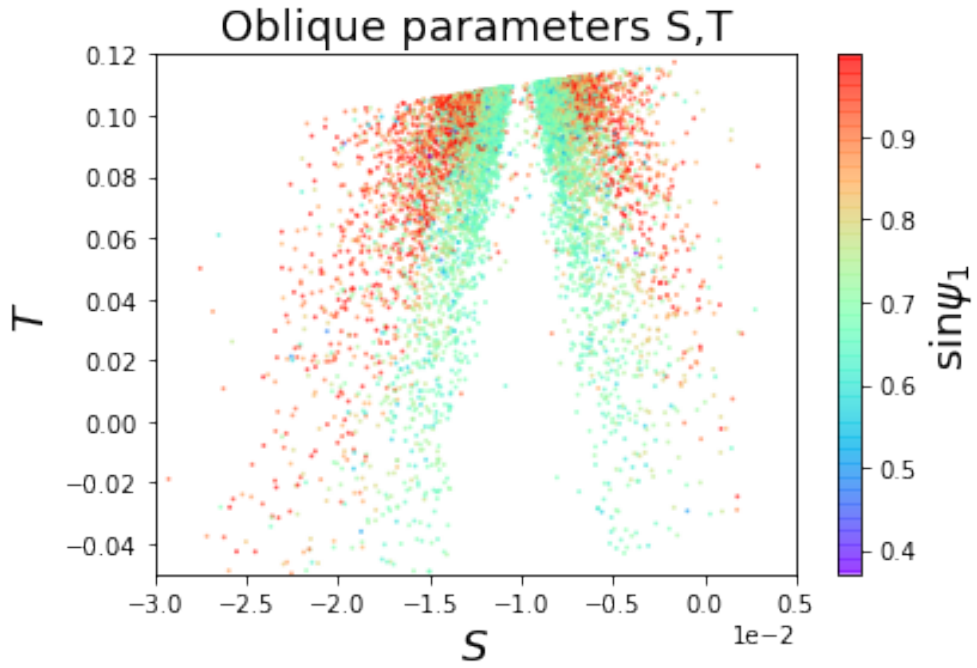

Figure 13: Values of $\sin\psi_1$, which have passed the HB/HS/EW-precision tests, mapped onto the space spanned by the oblique parameters S and T.

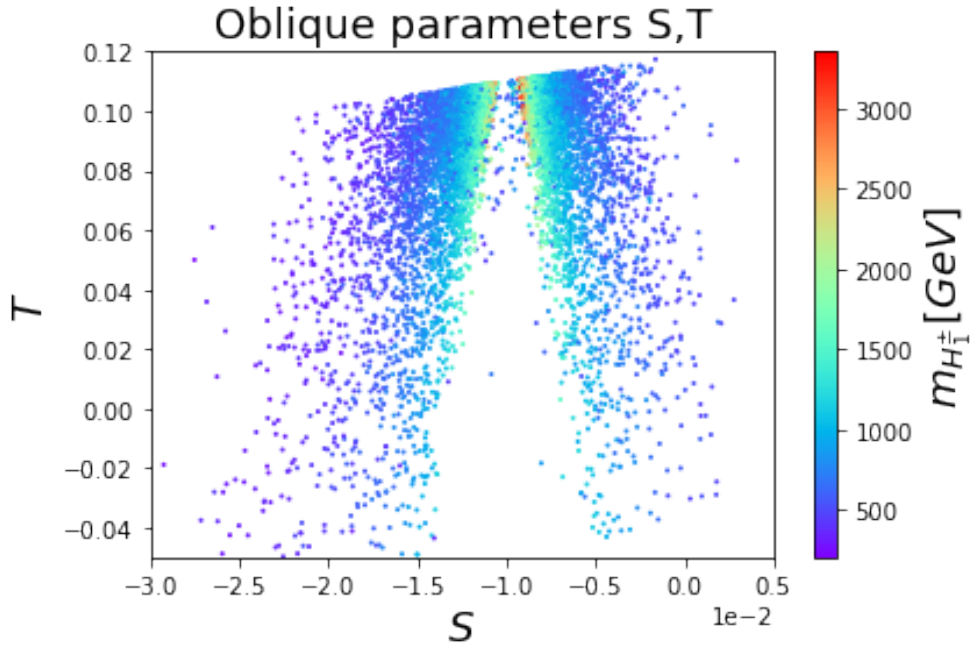

Figure 14: Masses of the lightest charged scalar $H_1^\pm$, which have passed the HB/HS/EW-precision tests, mapped onto the space spanned by the oblique parameters S and T.

scalars since their dependence is very similar to the one shown for $m_{H_1^\pm}$. In figures (15) we show the branching ratio of the decay $B \to X_s\gamma$, whose loop-level diagram was discussed in the 3HDM framework in section (3.5.3). Simultaneously, we also include figures (20) in the current discussion since both processes in (15) and (20) are described by the same transition $b \to s\gamma$. Since $b \to s\gamma$ takes place at loop level both in our 3HDM and in the SM (see table 1), the contribution mediated by the non-SM scalars is suppressed compared to the SM contribution due to large non-SM scalar masses or small Yukawa couplings. This is the case because the NP contribution to these processes (see diagram 7) is expected to be suppressed by the mass scale of non-SM scalars. From our results, we learn that small values of the angle ψ_1 and/or large masses of non-SM scalars, result in values of $B \to X_s\gamma$ and $B \to X_s\ell\bar{\ell}$ which are very close to the SM prediction. Furthermore, according to table 2, these branching ratios have been measured with experimental accuracies of 6.8% and 12%, respectively, which suggest that the transition $b \to s\gamma$ is most likely under control in our model. The splitting in figures (15) and (20) can be understood by looking at different ranges of the angle χ_3 which parametrizes the U_L^d matrix, as sketched in section (3.1). We have found that for values of χ_3 roughly below $\pi/2$, the value of $\mathcal{BR}(B \to X_s\gamma)$ is inferior to the SM prediction, and superior for greater values of the angle χ_3 within one period. Furthermore, the strong splitting for large values of ψ_1 (or equivalently light non-SM scalars) can be qualitatively understood as follows: according to section 3.5, light scalars lead to large NP contributions, therefore, although the angle χ_3 allows for almost vanishing Yukawa couplings, the light non-SM scalars increase the prediction of QFV

observables as their masses decrease. Finally, the two branches of points are due to the positive and negative values of $\cos\chi_3$ and $\sin\chi_3$ as χ_3 is varied from 0 to 2π.

In figures (16) we show the branching ratio of the process $B^0 \to \mu\overline{\mu}$. One interesting characteristic of the prediction of this process is the strong splitting between two values, whose center is not the SM prediction but a greater value instead. Between these two preferred values, namely ~ 1.07 and ~ 1.03 there is a gap where no point can be found. Also, contrary to the behavior of the process in figure (15), there is barely a spreading around these values, resulting in a pair of well-defined bands. Similar behavior is also present in the branching ratio of the decay $B_s \to \mu\overline{\mu}$ shown in figures (17), where two values are preferred. Nevertheless, the difference is that in the case of B_s the two bands are significantly spread around the SM prediction, in contrast to the case of B^0, where two well-defined bands lie above the SM prediction. In overall, the processes $B^0 \to \mu\overline{\mu}$ and $B_s \to \mu\overline{\mu}$ are in good agreement with the SM prediction and do not show any dangerous contribution that will, at first sight, violate the experimental accuracy reported in table 2.

The theoretical prediction for B mesons oscillations ΔM_{B_d} and ΔM_{B_s} in our model are presented in figures (18) and (19), respectively. The oscillations of the B meson set the strongest constraints on our model and to understand this, we need to keep in mind that ΔM_{B_d} and ΔM_{B_s} have been measured with great experimental accuracy, 0.35% and 0.11%, respectively, according to table 2. Additionally, our results present a set of points that are widely spread around the SM prediction. Although most of the points are, at first glance, in agreement with both experimental and theoretical estimations, a large number of parameters points will be excluded due to dangerous NP contributions in the $B_{d,s} - \overline{B}_{d,s}$ system. Nevertheless, this is no surprise: meson oscillations in our model are tree-level interactions mediated by neutral scalars $H_{2,3}$ while the SM contribution takes place only at loop-level, according to table 1. It is therefore expected that NP contributions win over SM contributions for some regions of the parameter space, as can be concluded from our results.

Lastly, the decay with a pair of neutrinos in the final states e.g. $K^+ \to \pi^+\nu\overline{\nu}$ is shown in figures (21). Although this decay does not impose stringent constraints on our model, it is included for completeness and is worth studying since it is a smoking gun for NP contributions, as discussed in section (2.5.1). This decay is described by the transition at quark level $s \to d\nu\overline{\nu}$, where the interaction is mediated by heavy charged scalars $H^{\pm}_{1,2}$ according to figure 2. Given the fact that an experimental accuracy of 65% is reported according to table 2, parameter space points of our model are very loosely constrained by this QFV observable and, most likely, only parameter points with values very close to $\sin\psi_1 = 1$ would lead to a prediction of the decay $K^+ \to \pi^+\nu\overline{\nu}$ that could generate tensions with the SM predictions.

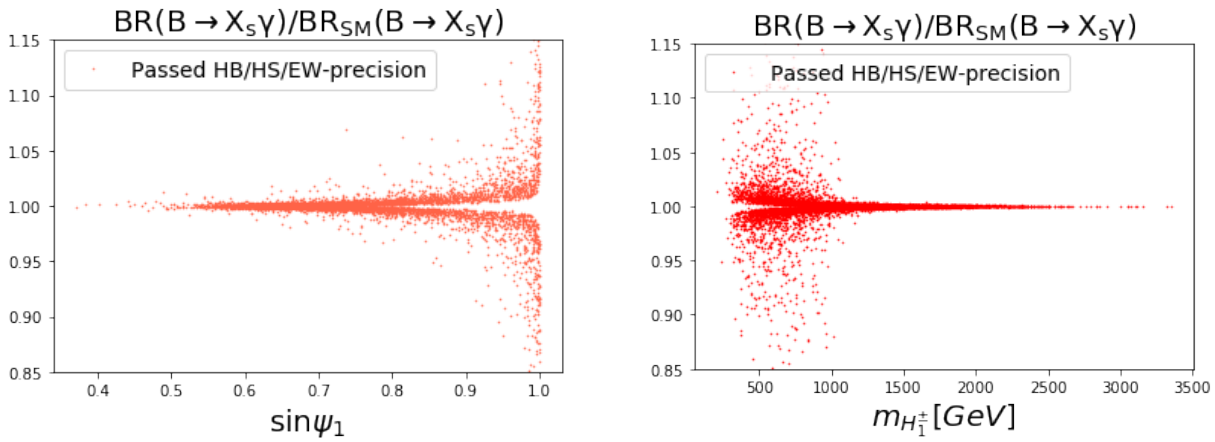

Figure 15: Estimation of the QFV observable $\mathcal{BR}(B \to X_s\gamma)$ normalized to the SM prediction of the parameter points that have passed the HB/HS/EW-precision tests. The left panel (orange) shows the dependence on $\sin\psi_1$, while the right panel (red) the dependence on the masses of the lightest charged scalar $H_1^\pm$.

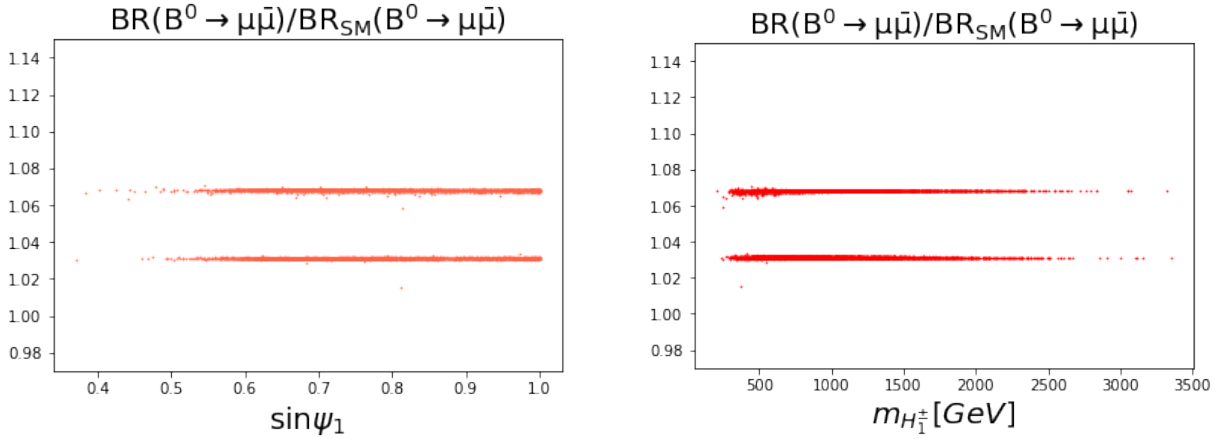

Figure 16: Estimation of the QFV observable $\mathcal{BR}(B^0 \to \mu\overline{\mu})$ normalized to the SM prediction of the parameter points that have passed the HB/HS/EW-precision tests.

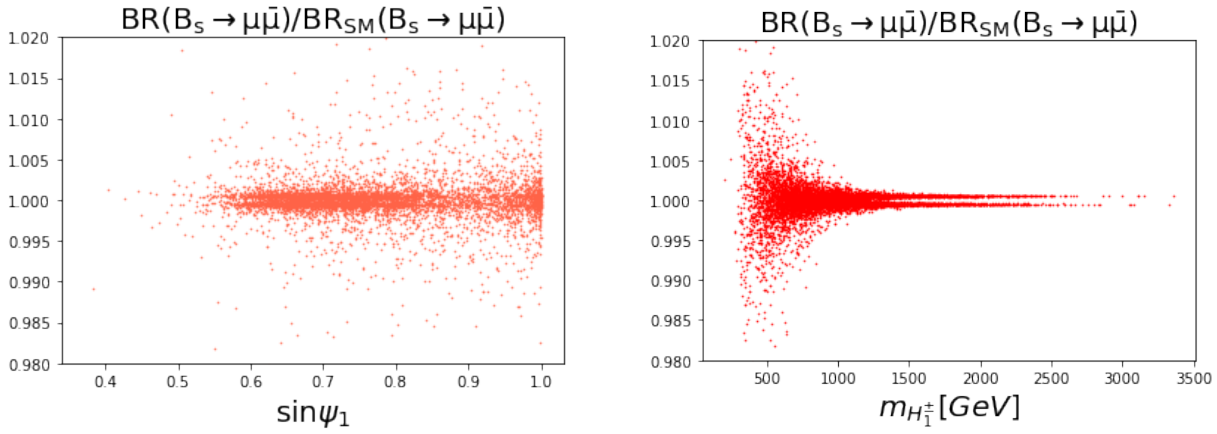

Figure 17: Estimation of the QFV observable $\mathcal{BR}(B_s \to \mu\bar{\mu})$ normalized to the SM prediction of the parameter points that have passed the HB/HS/EW-precision tests.

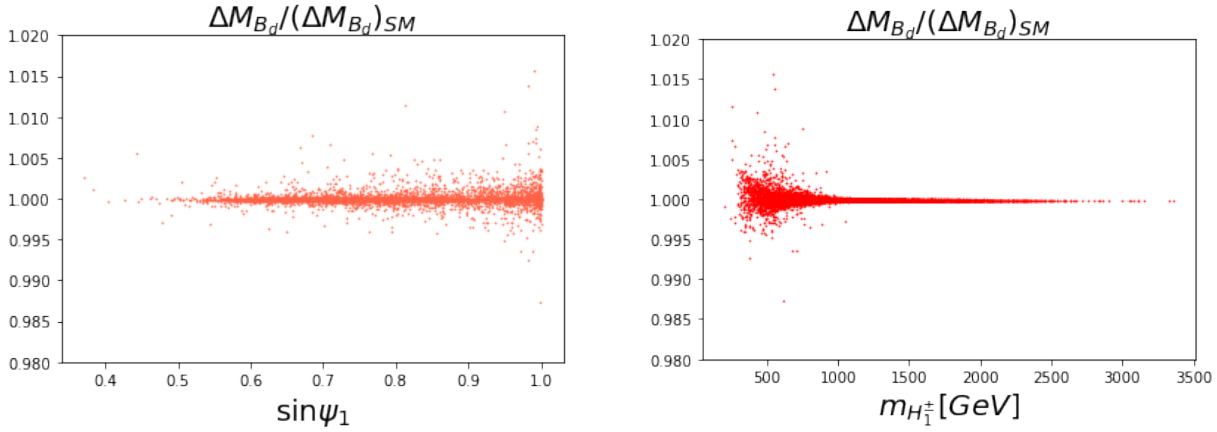

Figure 18: Estimation of the QFV observable ΔM_{B_d} normalized to the SM prediction of the parameter points that have passed the HB/HS/EW-precision tests.

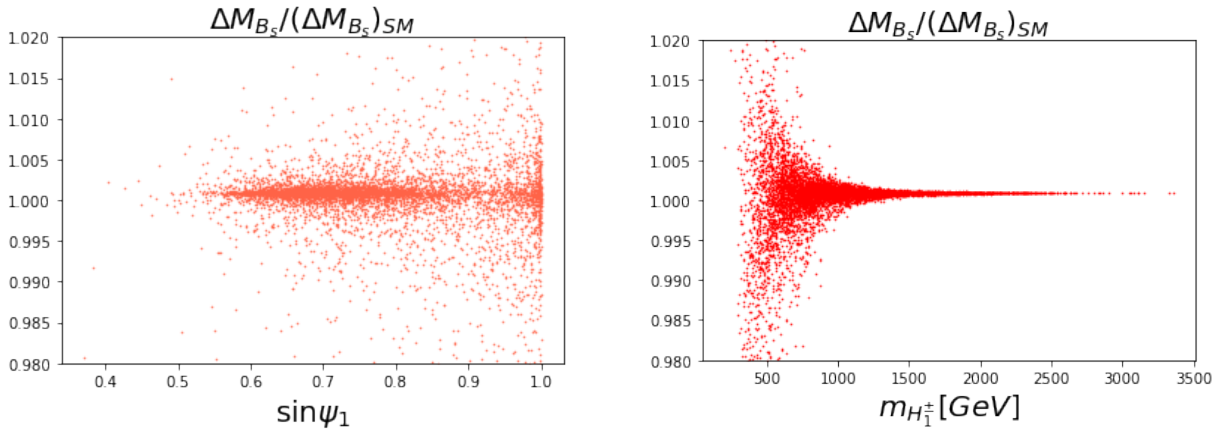

Figure 19: Estimation of the QFV observable ΔM_{B_s} normalized to the SM prediction of the parameter points that have passed the HB/HS/EW-precision tests.

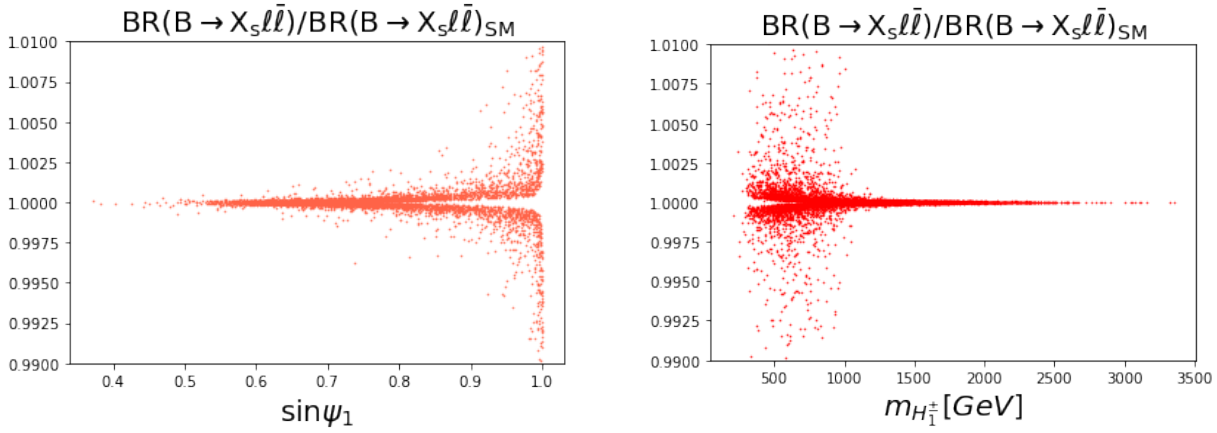

Figure 20: Estimation of the QFV observable $\mathcal{BR}(B \to X_s\ell\bar{\ell})$ normalized to the SM prediction of the parameter points that have passed the HB/HS/EW-precision tests.

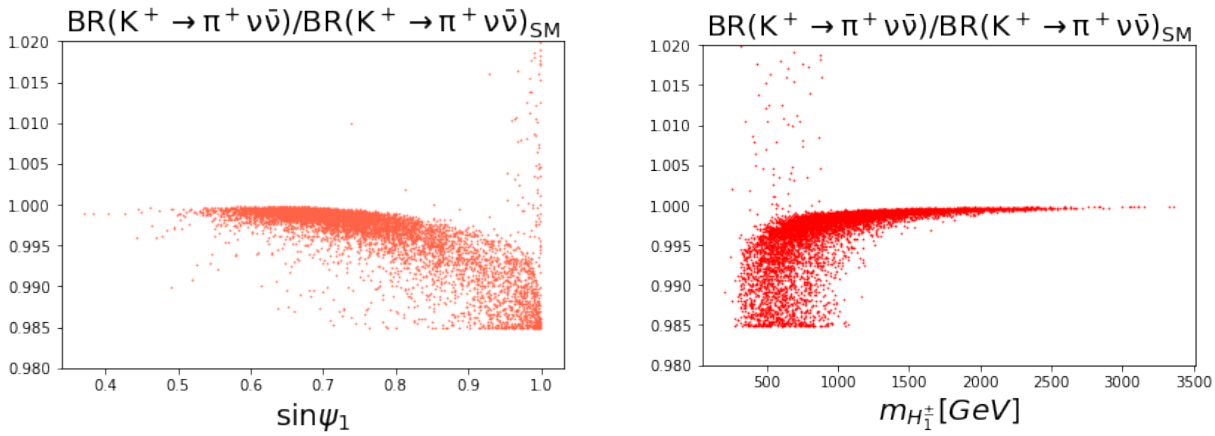

Figure 21: Estimation of the QFV observable $\mathcal{BR}(K^+ \to \pi^+ \nu\overline{\nu})$ normalized to the SM prediction of the parameter points that have passed the HB/HS/EW-precision tests.

5 Conclusions

We have studied the phenomenological consistency of a family-nonuniversal 3HDM with a softly broken U(1) $\times$ Z_2 family symmetry. The 3HDM model studied in this thesis aims to suppress potentially dangerous tree-level FCNCs mediated by non-standard scalar fields whose NP contribution could be sizable. Our implementation imposed conditions for alignment on the scalar sector to recover a SM-like Higgs boson while giving rise to heavier non-SM scalars. At a later stage, we have performed numerical analyses to confront experimental data coming from Higgs boson searches. To further constrain the parameter space of our model, EW precision tests were performed to ensure that NP contributions are within the allowed experimental bounds. Finally, predictions of QFV observables of the model were numerically estimated. We have found that our model respects a wide variety of QFV observables presented in section 4.2, where the B meson oscillations ΔM_{B_d} and ΔM_{B_s} set stringent constraints on our model.

Based on the discussion in section 4.2, we conclude that the 3HDM model studied in this thesis is capable of suppressing dangerous FCNCs mediated by non-SM scalars. Furthermore, some of the allowed exotic scalars are found to be relatively light indicating that the model succeeds in confronting flavour data even in the presence of scalars as light as 300 GeV. Hence, the studied 3HDM opens the door to direct searches for non-SM scalars at future runs of the LHC.

Acknowledgements

I am deeply indebted with my family for being the cornerstone of my personal and academic growth. Special thanks to my supervisor Roman Pasechnik and my co-supervisor Dipankar Das for their guidance throughout the project. Thanks to António Morais, João Pedro and Werner Porod for their essential contribution to the project and their lovely company in Lund. I am grateful to my officemates Robin and Ignacio for their amazing company during these past months. Also, many thanks to Joel Oredsson, Hugo Serodio and Astrid Ordell for their guidance at the beginning of the project. Equally grateful I am to all my friends at Fysicum, to my girlfriend Ayda and to my roommates Evelyn, Santiago, Natalia, Lulú, Javier and Ricardo for making Lund feel like home.

A Appendix A

Quartic terms λ_{1-10} and the soft-breaking parameter m_{23}^2 in terms of the scalar masses m_{125}, $m_{H_{2,3}}$, $m_{A^0_{1,2}}$, $m_{H^\pm_{1,2}}$, the VEV parameters ψ_1, ψ_2 and the angles $\delta_0, \delta_1, \delta_2$ that parametrize the scalar sector.

$$\begin{aligned}
\lambda_1 &= -(\csc^2\psi_1 \sec^2\psi_2(-32m_{125}^2\cos^2\psi_2\sin^2\psi_1 - 32(m_{H_2}^2(-(\cos\psi_1\sin\delta_0) \\
&\quad + \cos\delta_0\sin\psi_1\sin\psi_2)^2 + m_{H_2}^2(\cos\delta_0\cos\psi_1 + \sin\delta_0\sin\psi_1\sin\psi_2)^2)))/(64v^2) \qquad \text{(A.1)} \\
\lambda_2 &= (m_{125}^2 + \cot\psi_2(m_{H_2}^2\cos^2\delta_0\cot\psi_2 + m_{H_2}^2\cot\psi_2\sin^2\delta_0, \\
&\quad + \cos\psi_1\csc^2\psi_2(((m_{A_1^0}^2 - m_{A_2^0}^2)\cos\delta_1\cos\psi_2\csc\psi_1\sin\delta_1)/2 \\
&\quad - (\cos\psi_2\sec\psi_1(m_{A_2^0}^2\cos^2\delta_1 + m_{A_1^0}^2\sin^2\delta_1)\sin\psi_2)/2)))/(2v^2), \qquad \text{(A.2)} \\
\lambda_3 &= (m_{125}^2 + m_{H_2}^2\cos^2\delta_0\sec^2\psi_2\tan^2\psi_1 \\
&\quad + \sec\psi_1 3\sec^2\psi_2(((m_{A_1^0}^2 - m_{A_2^0}^2)\cos\delta_1\cos\psi_2\csc\psi_1\sin\delta_1)/2 \\
&\quad - (\cos\psi_2\sec\psi_1(m_{A_2^0}^2\cos^2\delta_1 + m_{A_1^0}^2\sin^2\delta_1)\sin\psi_2)/2)\tan\psi_2 \\
&\quad - m_{H_2}^2\sec\psi_2\sin(2\delta_0)\tan\psi_1\tan\psi_2 + m_{H_2}^2\sin^2\delta_0\tan^2\psi_2 \\
&\quad + m_{H_2}^2(\sec\psi_2\sin\delta_0\tan\psi_1 + \cos\delta_0\tan\psi_2)^2)/(2v^2), \qquad \text{(A.3)} \\
\lambda_4 &= (2m_{125}^2 - 2m_{H_2}^2\cos^2\delta_0 + 4m_{H_2^\pm}\cos^2\delta_2 - m_{H_2}^2(2\sin^2\delta_0 \\
&\quad + \cot\psi_1\csc\psi_2\sin(2\delta_0)) + 4m_{H_1^\pm}\sin^2\delta_2 + \cot\psi_1\csc\psi_2(m_{H_2}^2\sin(2\delta_0) \\
&\quad + 2(m_{H_1^\pm} - m_{H_2^\pm})\sin(2\delta_2)))/(2v^2), \qquad \text{(A.4)} \\
\lambda_5 &= (16m_{125}^2 + m_{H_2}^2(-1 - 7\sec^2\psi_2 + \cos(2\delta_0)(8 - 16\sec^2\psi_2) \\
&\quad + 8\cos(2\psi_1)\csc\psi_1\sec\psi_1\sec\psi_2\sin(2\delta_0)\tan\psi_2 + 7\tan^2\psi_2) \\
&\quad + 4(8m_{H_2^\pm}(\cos^2\delta_2 - \cos(2\delta_2)\sec^2\psi_2) + 8m_{H_1^\pm}(\cos(2\delta_2)\sec^2\psi_2 \\
&\quad + \sin^2\delta_2) + 4(-m_{H_1^\pm} + m_{H_2^\pm})\cos(2\psi_1)\csc\psi_1\sec\psi_1\sec\psi_2\sin(2\delta_2)\tan\psi_2 \\
&\quad + m_{H_2}^2(\sec\psi_2((-1 + 3\cos(2\delta_0))\sec\psi_2 - 2\cos(2\psi_1)\csc\psi_1\sec\psi_1\sin(2\delta_0)\tan\psi_2) \\
&\quad + 2\cos^2\delta_0(-1 + \tan^2\psi_2))))/(16v^2), \qquad \text{(A.5)} \\
\lambda_6 &= (2m_{125}^2 - 2m_{H_2}^2\cos^2\delta_0 + 4m_{H_2^\pm}\cos^2\delta_2 - 2m_{H_2}^2\sin^2\delta_0 + 4m_{H_1^\pm}\sin^2\delta_2 \\
&\quad + 2\csc\psi_2\sec\psi_1\sec\psi_2(((m_{A_1^0}^2 - m_{A_2^0}^2)\cos\delta_1\cos\psi_2\csc\psi_1\sin\delta_1)/2 \\
&\quad - (\cos\psi_2\sec\psi_1(m_{A_2^0}^2\cos^2\delta_1 + m_{A_1^0}^2\sin^2\delta_1)\sin\psi_2)/2) \\
&\quad + \csc\psi_2((m_{H_2}^2 - m_{H_2}^2)\sin(2\delta_0) + 2(-m_{H_1^\pm} + m_{H_2^\pm})\sin(2\delta_2))\tan\psi_1)/(2v^2), \qquad \text{(A.6)} \\
\lambda_7 &= (m_{H_1^\pm}(-2\sin^2\delta_2 - \cot\psi_1\csc\psi_2\sin(2\delta_2)) + m_{H_2^\pm}(-2\cos^2\delta_2 \\
&\quad + \cot\psi_1\csc\psi_2\sin(2\delta_2)))/v^2, \qquad \text{(A.7)}
\end{aligned}$$

$$
\begin{aligned}
\lambda_8 = &-(m_{H_2^\pm} + m_{H_2^\pm}\cos^2\delta_2 + 3m_{H_1^\pm}\sec^2\psi_2 + 3m_{H_2^\pm}\sec^2\psi_2 - 4m^2_{A_1^0}\cos^2\delta_1\sec^2\psi_2 \\
&+ 5m_{H_1^\pm}\cos^2\delta_2\sec^2\psi_2 - 5m_{H_2^\pm}\cos^2\delta_2\sec^2\psi_2 - 4m^2_{A_2^0}\sec^2\psi_2\sin^2\delta_1 \\
&+ 2m_{H_1^\pm}\sin^2\delta_2 - m_{H_2^\pm}\sin^2\delta_2 - 5m_{H_1^\pm}\sec^2\psi_2\sin^2\delta_2 + 5m_{H_2^\pm}\sec^2\psi_2\sin^2\delta_2 \\
&- 4\csc\psi_1\sec\psi_2((m_{H_1^\pm} - m_{H_2^\pm})\cos(2\psi_1)\sec\psi_1\sin(2\delta_2) \\
&+ \sec\psi_2\sin^2\psi_1(((m^2_{A_1^0} - m^2_{A_2^0})\cos\delta_1\cos\psi_2\csc\psi_1\sin\delta_1)/2 \\
&- (\cos\psi_2\sec\psi_1(m^2_{A_2^0}\cos\delta_1^2 + m^2_{A_1^0}\sin^2\delta_1)\sin\psi_2)/2)\tan\psi_1)\tan\psi_2 \\
&- 6(m_{H_2^\pm}\cos^2\delta_2 + m_{H_1^\pm}\sin^2\delta_2)\tan\psi_2^2)/(4v^2), \qquad \text{(A.8)} \\
\lambda_9 = &(-2(\csc\psi_2\sec\psi_1\sec\psi_2(((m^2_{A_1^0} - m^2_{A_2^0})\cos\delta_1\cos\psi_2\csc\psi_1\sin\delta_1)/2 \\
&- (\cos\psi_2\sec\psi_1(m^2_{A_2^0}\cos^2\delta_1 + m^2_{A_1^0}\sin^2\delta_1)\sin\psi_2)/2) + m_{H_1^\pm}\sin\delta_2(\sin\delta_2 \\
&- \cos\delta_2\csc\psi_2\tan\psi_1) + m_{H_2^\pm}\cos\delta_2(\cos\delta_2 + \csc\psi_2\sin\delta_2\tan\psi_1)))/v^2, \qquad \text{(A.9)} \\
\lambda_{10} = &-(\sec^2\psi_2(m^2_{A_1^0}\cos^2\delta_1 + m^2_{A_2^0}\sin^2\delta_1 + \\
&+ \sin\psi_1(((m^2_{A_1^0} - m^2_{A_2^0})\cos\delta_1\cos\psi_2\csc\psi_1\sin\delta_1)/2 \\
&- (\cos\psi_2\sec\psi_1(m^2_{A_2^0}\cos^2\delta_1 + m^2_{A_1^0}\sin^2\delta_1)\sin\psi_2)/2)\tan\psi_1\tan\psi_2))/(2v^2), \qquad \text{(A.10)} \\
m^2_{23} = &\, m^2_{A_1^0}((\cos\psi_2\sec\psi_1\sin\psi_2)/(\tan\psi_1\sin\psi_2\cot\delta_1 - 1)). \qquad \text{(A.11)}
\end{aligned}
$$

B Appendix B

Interaction vertices of heavier non-standard neutral scalars with quarks in the down sector where most of the FCNCs are expected.

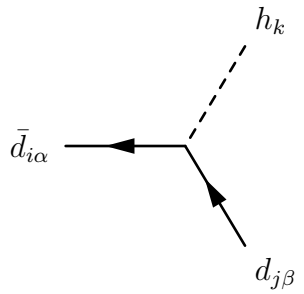

$$
\begin{aligned}
&- i\frac{1}{\sqrt{2}}\delta_{\alpha\beta}\Big(\sum_{b=1}^{3}U^{d,*}_{L,jb}\sum_{a=1}^{3}U^{d,*}_{R,ia}Y^{d}_{1,ab}Z^{H}_{k1}+\sum_{b=1}^{3}U^{d,*}_{L,jb}\sum_{a=1}^{3}U^{d,*}_{R,ia}Y^{d}_{2,ab}Z^{H}_{k2}\\
&+\sum_{b=1}^{3}U^{d,*}_{L,jb}\sum_{a=1}^{3}U^{d,*}_{R,ia}Y^{d}_{3,ab}Z^{H}_{k3}\Big)\Big(\frac{1-\gamma_5}{2}\Big)\\
&+\ -i\frac{1}{\sqrt{2}}\delta_{\alpha\beta}\Big(\sum_{b=1}^{3}\sum_{a=1}^{3}Y^{d,*}_{1,ab}U^{d}_{R,ja}U^{d}_{L,ib}Z^{H}_{k1}+\sum_{b=1}^{3}\sum_{a=1}^{3}Y^{d,*}_{2,ab}U^{d}_{R,ja}U^{d}_{L,ib}Z^{H}_{k2}\\
&+\sum_{b=1}^{3}\sum_{a=1}^{3}Y^{d,*}_{3,ab}U^{d}_{R,ja}U^{d}_{L,ib}Z^{H}_{k3}\Big)\Big(\frac{1+\gamma_5}{2}\Big)
\end{aligned}
\tag{B.1}
$$

Interaction vertices of heavier non-standard charged scalars with up- and down-type quarks.

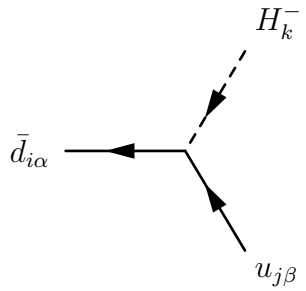

$$
\begin{aligned}
&- i\delta_{\alpha\beta}\Big(\sum_{b=1}^{3}U^{u,*}_{L,jb}\sum_{a=1}^{3}U^{d,*}_{R,ia}Y^{d}_{1,ab}Z^{+}_{k1}+\sum_{b=1}^{3}U^{u,*}_{L,jb}\sum_{a=1}^{3}U^{d,*}_{R,ia}Y^{d}_{2,ab}Z^{+}_{k2}\\
&+\sum_{b=1}^{3}U^{u,*}_{L,jb}\sum_{a=1}^{3}U^{d,*}_{R,ia}Y^{d}_{3,ab}Z^{+}_{k3}\Big)\Big(\frac{1-\gamma_5}{2}\Big)\\
&+\ i\delta_{\alpha\beta}\Big(\sum_{b=1}^{3}\sum_{a=1}^{3}Y^{u,*}_{1,ab}U^{u}_{R,ja}U^{d}_{L,ib}Z^{+}_{k1}+\sum_{b=1}^{3}\sum_{a=1}^{3}Y^{u,*}_{2,ab}U^{u}_{R,ja}U^{d}_{L,ib}Z^{+}_{k2}\\
&+\sum_{b=1}^{3}\sum_{a=1}^{3}Y^{u,*}_{3,ab}U^{u}_{R,ja}U^{d}_{L,ib}Z^{+}_{k3}\Big)\Big(\frac{1+\gamma_5}{2}\Big)
\end{aligned}
\tag{B.2}
$$

C Appendix C

The $X_0(x)$ contribution to the $X(x)$ function for the effective NLO Hamiltonian inducing $K^+ \to \pi^+\nu\overline{\nu}$ is given by [49]

$$
X_0(x) = \frac{x}{8}\Big[-\frac{2+x}{1-x}+\frac{3x-6}{(1-x)^2}\ln x\Big], \tag{C.1}
$$

while the $X_1(x)$ QCD correction is [50]

$$X_1(x) = -\frac{23x + 5x^2 - 4x^3}{3(1-x)^2} + \frac{x - 11x^2 + x^3 + x^4}{(1-x)^3 \ln x} + \frac{8x + 4x^2 + x^3 - x^4}{2(1-x)^3} \ln^2 x - \frac{4x - x^3}{(1-x)^2} L_2(1-x) + 8x \frac{\partial X_0(x)}{\partial x} \ln x_\mu, \tag{C.2}$$

where $x_\mu = \mu^2/M_W^2$ with $\mu = \mathcal{O}(m_t)$ and the function L_2 is defined as

$$L_2(1-x) \int_1^x dt \frac{\ln t}{1-t}. \tag{C.3}$$

The NLO contribution to the effective Hamiltonian in (2.31) is computed from the renormalization group calculation in [49] and is given in terms of the following coefficients

$$X_{NL}^{\ell} = C_{NL} - 4B_{NL}^{(1/2)}, \tag{C.4}$$

where C_{NL} and $B_{NL}^{(1/2)}$ carry the Z^0-penguin and the box diagram contribution, respectively. Consequently, we have that

$$C_{NL} = \frac{x(m)}{32}\Bigg[\Big(\frac{48}{7}K_+ \frac{24}{11}K_- - \frac{696}{77}K_{33}\Big)\Big(\frac{4\pi}{\alpha_s \mu} + \frac{15212}{1875}(1 - K_c^{-1})\Big) + \Big(1 - \ln\frac{\mu^2}{m^2}\Big)(16K_+ - 8K_-) - \frac{1176244}{13125}K_+ - \frac{2302}{6875}K_- + \frac{3529184}{48125}K_{33} + K\Big(\frac{56248}{4375}K_+ - \frac{81448}{6875}K + \frac{4563698}{144375}K_{33}\Big)\Bigg], \tag{C.5}$$

where

$$K = \frac{\alpha_s(M_W)}{\alpha_s(\mu)}, \;\; K_c = \frac{\alpha_s(\mu)}{\alpha_s(m)}, \quad K_+ = K^{6/25}, \;\; K_- = K^{-12/25}, \;\; K_{33} = K^{-1/25} \tag{C.6}$$

and $B_{NL}^{(1/2)}$ is given by

$$B_{NL}^{(1/2)} = \frac{x(m)}{4} K_c^{24/25}\Big[3(1-K_2)\Big(\frac{4\pi}{\alpha_s(\mu)} + \frac{15212}{1875}(1 - K_c^{-1})\Big) - \ln\frac{\mu^2}{m^2} - \frac{r \ln r}{1-r} - \frac{305}{12} + \frac{15212}{625}K_2 + \frac{15581}{7500}K K_2\Big], \tag{C.7}$$

here $K_2 = K^{-1/25}$, $m = m_c$, $r = m_\ell^2/m_c^2(\mu)$ and m_ℓ is the lepton mass. The explicit terms $\ln \mu^2/m^2$ in the coefficients (C.5) and (C.7) cancel the dependence on μ of the leading terms. For more details, see [49] and references therein.

D Appendix D

The SM one-loop functions $Y_0(x_t)$ and $Z_0(x_t)$ needed to compute the SM value of the Wilson coefficients in (2.38) are given by [25],

$$Y_0(x_t) = \frac{x_t}{8}\Big(\frac{x_t-4}{x_t-1} + \frac{3x_t \log x_t}{(x_t-1)^2}\Big), \tag{D.1}$$

$$Z_0(x_t) = -\frac{1}{9}\log x_t + \frac{18x_t^4 - 163x_t^3 + 259x_t^2 - 108x_t}{144(x_t-1)^3} + \frac{32x_t^4 - 38x_t^3 - 15x_t^2 + 18x_t}{72(x-1)^4}\log x_t, \tag{D.2}$$

where, as before, x_t is defined as $x_t = m_t^2/M_W^2$.

References

[1] ATLAS collaboration, *Observation of a new particle in the search for the Standard Model Higgs boson with the ATLAS detector at the LHC*, *Phys. Lett.* **B716** (2012) 1 [1207.7214].

[2] I. P. Ivanov, *Building and testing models with extended Higgs sectors*, *Prog. Part. Nucl. Phys.* **95** (2017) 160 [1702.03776].

[3] G. C. Branco, P. M. Ferreira, L. Lavoura, M. N. Rebelo, M. Sher and J. P. Silva, *Theory and phenomenology of two-Higgs-doublet models*, *Phys. Rept.* **516** (2012) 1 [1106.0034].

[4] F. J. Botella, G. C. Branco and M. N. Rebelo, *Minimal Flavour Violation and Multi-Higgs Models*, *Phys. Lett.* **B687** (2010) 194 [0911.1753].

[5] J. E. Camargo-Molina, T. Mandal, R. Pasechnik and J. Wessén, *Heavy charged scalars from $c\bar{s}$ fusion: A generic search strategy applied to a 3HDM with* $\mathrm{U}(1) \times \mathrm{U}(1)$ *family symmetry*, *JHEP* **03** (2018) 024 [1711.03551].

[6] M. Srednicki, *Quantum Field Theory*. Cambridge University Press, 2007.

[7] S. Willenbrock, *Symmetries of the standard model*, in *Physics in D ¿= 4. Proceedings, Theoretical Advanced Study Institute in elementary particle physics, TASI 2004, Boulder, USA, June 6-July 2, 2004*, pp. 3–38, 2004, hep-ph/0410370.

[8] G. Kane, *Modern Elementary Particle Physics*. Cambridge University Press, 2007.

[9] Particle Data Group collaboration, *Review of Particle Physics*, *Chin. Phys.* **C40** (2016) 100001.

[10] N. Cabibbo, *Unitary symmetry and leptonic decays*, *Phys. Rev. Lett.* **10** (1963) 531.

[11] M. Kobayashi and T. Maskawa, *CP-Violation in the Renormalizable Theory of Weak Interaction*, *Progress of Theoretical Physics* **49** (1973) 652 [http://oup.prod.sis.lan/ptp/article-pdf/49/2/652/5257692/49-2-652.pdf].

[12] L. Wolfenstein, *Parametrization of the kobayashi-maskawa matrix*, *Phys. Rev. Lett.* **51** (1983) 1945.

[13] M. Blanke, *Introduction to Flavour Physics and CP Violation*, *CERN Yellow Rep. School Proc.* **1705** (2017) 71 [1704.03753].

[14] C. Jarlskog, *A basis independent formulation of the connection between quark mass matrices, cp violation and experiment*, *Zeitschrift für Physik C Particles and Fields* **29** (1985) 491.

[15] S. L. Glashow, J. Iliopoulos and L. Maiani, *Weak interactions with lepton-hadron symmetry*, *Phys. Rev. D* **2** (1970) 1285.

[16] A. J. Buras, *Flavour Theory: 2009*, *PoS* **EPS-HEP2009** (2009) 024 [0910.1032].

[17] X.-G. He, G. Valencia and K. Wong, *Constraints on new physics from $K \to \pi\nu\overline{\nu}$*, *The European Physical Journal C* **78** (2018) 472.

[18] G. Buchalla, A. J. Buras and M. E. Lautenbacher, *Weak decays beyond leading logarithms*, *Rev. Mod. Phys.* **68** (1996) 1125 [hep-ph/9512380].

[19] A. J. Buras, R. Fleischer, S. Recksiegel and F. Schwab, *Anatomy of prominent B and K decays and signatures of CP violating new physics in the electroweak penguin sector*, *Nucl. Phys.* **B697** (2004) 133 [hep-ph/0402112].

[20] H. Albrecht, A. Andam, U. Binder, P. Böckmann, R. Gläser, G. Harder et al., *Observation of b0-b0 mixing*, *Physics Letters B* **192** (1987) 245 .

[21] Belle Collaboration collaboration, *Observation of large CP violation in the neutral B meson system*, *Phys. Rev. Lett.* **87** (2001) 091802.

[22] BABAR Collaboration collaboration, *Observation of CP violation in the b^0 meson system*, *Phys. Rev. Lett.* **87** (2001) 091801.

[23] CDF collaboration, *Observation of $B_s^0 - \bar{B}_s^0$ Oscillations*, *Phys. Rev. Lett.* **97** (2006) 242003 [hep-ex/0609040].

[24] LHCb collaboration, *Measurement of the $B_s^0 - \bar{B}_s^0$ oscillation frequency Δm_s in $B_s^0 \to D_s^-(3)\pi$ decays*, *Phys. Lett.* **B709** (2012) 177 [1112.4311].

[25] A. J. Buras, F. De Fazio, J. Girrbach, R. Knegjens and M. Nagai, *The Anatomy of Neutral Scalars with FCNCs in the Flavour Precision Era*, *JHEP* **06** (2013) 111 [1303.3723].

[26] F. J. Botella, G. C. Branco, A. Carmona, M. Nebot, L. Pedro and M. N. Rebelo, *Physical Constraints on a Class of Two-Higgs Doublet Models with FCNC at tree level*, *JHEP* **07** (2014) 078 [1401.6147].

[27] G. Buchalla and A. J. Buras, *The rare decays $K \to \pi\nu\bar{\nu}$, $B \to X\nu\bar{\nu}$ and $B \to l^+l^-$: An Update*, *Nucl. Phys.* **B548** (1999) 309 [hep-ph/9901288].

[28] M. Misiak and J. Urban, *QCD corrections to FCNC decays mediated by Z penguins and W boxes*, *Phys. Lett.* **B451** (1999) 161 [hep-ph/9901278].

[29] G. C. Branco, W. Grimus and L. Lavoura, *Relating the scalar flavor changing neutral couplings to the CKM matrix*, *Phys. Lett.* **B380** (1996) 119 [hep-ph/9601383].

[30] F. Staub, *Exploring new models in all detail with SARAH*, *Adv. High Energy Phys.* **2015** (2015) 840780 [1503.04200].

[31] D. Das and I. Saha, *Alignment limit in three Higgs-doublet models*, 1904.03970.

[32] V. Keus, S. F. King and S. Moretti, *Three-Higgs-doublet models: symmetries, potentials and Higgs boson masses*, *JHEP* **01** (2014) 052 [1310.8253].

[33] M. Gell-Mann, *A Schematic Model of Baryons and Mesons*, *Phys. Lett.* **8** (1964) 214.

[34] S. L. Glashow, J. Iliopoulos and L. Maiani, *Weak interactions with lepton-hadron symmetry*, *Phys. Rev. D* **2** (1970) 1285.

[35] M. Kobayashi and T. Maskawa, *CP-Violation in the Renormalizable Theory of Weak Interaction*, *Progress of Theoretical Physics* **49** (1973) 652 [http://oup.prod.sis.lan/ptp/article-pdf/49/2/652/5257692/49-2-652.pdf].

[36] A. J. Buras, *A 1993 look at the lower bound on the top quark mass from CP violation*, *Phys. Lett.* **B317** (1993) 449 [hep-ph/9307318].

[37] P. M. Ferreira, L. Lavoura, J. P. Silva and L. Lavoura, *A Soft origin for CKM-type CP violation*, *Phys. Lett.* **B704** (2011) 179 [1102.0784].

[38] J. Brod and M. Gorbahn, *Next-to-Next-to-Leading-Order Charm-Quark Contribution to the CP Violation Parameter $epsilon_K and Delta M_K$*, Phys. Rev. Lett.108(2012)121801[1108.2036].

[39] P. Bechtle, S. Heinemeyer, O. Stal, T. Stefaniak and G. Weiglein, Applying Exclusion Likelihoods from LHC Searches to Extended Higgs Sectors, Eur. Phys. J. ***C75*** *(2015) 421 [1507.06706].*

[40] P. Bechtle, S. Heinemeyer, O. Stål, T. Stefaniak and G. Weiglein, HiggsSignals: Confronting arbitrary Higgs sectors with measurements at the Tevatron and the LHC, Eur. Phys. J. ***C74*** *(2014) 2711 [1305.1933].*

[41] W. Porod, SPheno, a program for calculating supersymmetric spectra, SUSY particle decays and SUSY particle production at e+ e- colliders, Comput. Phys. Commun. ***153*** *(2003) 275 [hep-ph/0301101].*

[42] W. Porod and F. Staub, SPheno 3.1: Extensions including flavour, CP-phases and models beyond the MSSM, Comput. Phys. Commun. ***183*** *(2012) 2458 [1104.1573].*

[43] M. E. Peskin and T. Takeuchi, Estimation of oblique electroweak corrections, Phys. Rev. ***D46*** *(1992) 381.*

[44] R. Coimbra, M. O. P. Sampaio and R. Santos, ScannerS: Constraining the phase diagram of a complex scalar singlet at the LHC, Eur. Phys. J. ***C73*** *(2013) 2428 [1301.2599].*

[45] M. Baak, M. Goebel, J. Haller, A. Hoecker, D. Ludwig, K. Moenig et al., Updated Status of the Global Electroweak Fit and Constraints on New Physics, Eur. Phys. J. ***C72*** *(2012) 2003 [1107.0975].*

[46] D. M. Straub, flavio: a Python package for flavour and precision phenomenology in the Standard Model and beyond, *1810.08132.*

[47] Z.-z. Xing, H. Zhang and S. Zhou, Updated Values of Running Quark and Lepton Masses, Phys. Rev. ***D77*** *(2008) 113016 [0712.1419].*

[48] W. Porod, F. Staub and A. Vicente, A Flavor Kit for BSM models, Eur. Phys. J. ***C74*** *(2014) 2992 [1405.1434].*

[49] T. Inami and C. S. Lim, Effects of Superheavy Quarks and Leptons in Low-Energy Weak Processes KL, K++ and K0K0, Progress of Theoretical Physics ***65*** *(1981) 297 [http://oup.prod.sis.lan/ptp/article-pdf/65/1/297/5252099/65-1-297.pdf].*

[50] G. Buchalla and A. J. Buras, The rare decays k â ÏÎœÎœâ, b â xÎœÎœâ and b â l+lâ: an update, Nuclear Physics B ***548*** *(1999) 309 .*